

Wavelets

Andreas de Vries

FH Südwestfalen University of Applied Sciences, Haldener Straße 182, D-58095 Hagen, Germany

e-Mail: de-vries.andreas@fh-swf.de

Version: September 4, 2006; supplemented: March 1, 2021

Contents

1	Introduction	2
2	Daubechies wavelets	2
2.1	Dyadic numbers	7
2.2	Properties of Daubechies scaling functions	8
3	The fast Daubechies wavelet transform	9
3.1	Fast Inverse Daubechies Wavelet Transformation	12
4	General approach to wavelets	13
4.1	The Fourier transformation	14
4.2	Basic properties of wavelets	14
4.2.1	Wavelets and subband filters	16
4.3	Orthonormal wavelet packets	18
4.4	Biorthogonal wavelets	19
4.4.1	The one-dimensional case	20
4.4.2	The two-dimensional case	23
4.5	Malvar-Wilson wavelets	24
5	Wavelet transformation	26
5.1	The image space of a wavelet transformation	28
6	Sweldens' lifting scheme	29
7	Chirplets and the wavelet transformation	29
8	Vision	31
8.1	Marr's program	32
8.2	Edge recognition by zero-crossings	33
8.3	Mallat's algorithm	34
8.3.1	Mallat's algorithm in two dimensions	35

1 Introduction

Wavelet methods constitute the underpinning of a new comprehension of time-frequency analysis, or “space-wavenumber” analysis. They have emerged independently within different scientific branches of study until all these different viewpoints have been subsumed under the common terms of “wavelets” and “time-scale analysis”, or “scale-space-analysis” in the context of image processing.

Wavelet theory is closely connected to the Fourier transformation. In turn, the continuous wavelet transformation is an integral transformation similar to the Fourier transformation. But whereas the Fourier transformation analyzes the *global* regularity of a function, the wavelet transform analyzes the *pointwise* regularity of a function.¹ Wavelet theory involves representing general functions in terms of simpler, fixed building blocks at different scales and positions.

The present essay gives a short introduction into the theory of wavelets and some of its applications. It is organized as follows. First the important class of Daubechies wavelets is considered. They were developed by Ingrid Daubechies at the end of the 1980’s and represent a new kind of functions. They are frequently used in applications. Subsequently, the fast Daubechies transformation is introduced, a special discrete wavelet transformation basing on the Daubechies wavelets. Having this concrete examples in mind, then the approach to general wavelets and the wavelet transformation is given, before Sweldens’ lifting scheme, as a method to compute a discrete wavelet transform without explicit knowledge of the underlying wavelet, is described and some applications of wavelets to the related chirplets and to the theory of the human vision are considered.

2 Daubechies wavelets

Definition 2.1 For $N \in \mathbb{N}$, a *Daubechies wavelet* of class D-2N is a function $\psi = {}_N\psi \in L^2(\mathbb{R})$ defined by

$$\psi(x) := \sqrt{2} \sum_{k=0}^{2N-1} (-1)^k h_{2N-1-k} \varphi(2x - k), \quad (1)$$

where $h_0, \dots, h_{2N-1} \in \mathbb{R}$ are the constant *filter coefficients* satisfying the conditions

$$\sum_{k=0}^{N-1} h_{2k} = \frac{1}{\sqrt{2}} = \sum_{k=0}^{N-1} h_{2k+1}, \quad (2)$$

as well as, for $l = 0, 1, \dots, N-1$,

$$\sum_{k=2l}^{2N-1+2l} h_k h_{k-2l} = \begin{cases} 1 & \text{if } l = 0, \\ 0 & \text{if } l \neq 0, \end{cases} \quad (3)$$

and where $\varphi = {}_N\varphi : \mathbb{R} \rightarrow \mathbb{R}$ is the (*Daubechies*) *scaling function* (sometimes also “*scalet*” or “*father wavelet*”), given by the recursion equation

$$\varphi(x) = \sqrt{2} \sum_{k=0}^{2N-1} h_k \varphi(2x - k) \quad (4)$$

and obeying

$$\varphi(x) = 0 \quad \text{for } x \in \mathbb{R} \setminus [0, 2N - 1[. \quad (5)$$

¹http://cas.ensmp.fr/~chaplais/Wavetour_presentation/Regularite/Regularity.html

as well as

$$\int_{\mathbb{R}} \varphi(2x-k) \varphi(2x-l) dx = 0 \quad \text{for } k \neq l. \quad (6)$$

See [2, 3]. □

The first basic problem to construct Daubechies wavelets is the determination of the coefficients h_0, \dots, h_{2N-1} which admit a nonvanishing scaling function φ satisfying (4). Note that there are N equations given by the orthonormality conditions (3). Together with (2) this gives in total $N+2$ equations for the $2N$ filter coefficients h_k . Hence, for $N=1$, they are overdetermined, for $N=2$ they are unique (if they exist), and for $N>2$ they are underdetermined. However, once the filter coefficients are given, an elegant proof [8, Cor. 8.9], with the aid of the Fourier transformation of the corresponding recursion operator,² demonstrates the existence and uniqueness of a function φ satisfying (4) and the normalization condition $\int_{\mathbb{R}} \varphi = 1$, for a given sequence of h_0, \dots, h_{2N-1} .

The usual way, however, is the other way round: to first define the scaling function φ , and then to derive the filter coefficients. The general procedure will be outlined in Section 4.2, see Eq. (62).

Example 2.2 (*D2 wavelet, or Haar wavelet*) Let $N=1$ and $h_0 = 1/\sqrt{2}$, $h_1 = 1/\sqrt{2}$. Then the function with the initial values $\varphi(0) = 1$, $\varphi(k) = 0$ for $k \in \mathbb{Z}$, $k \neq 0$, determines the unique scaling function. Eq. (4) then reads simply $\varphi(x) = \varphi(2x) + \varphi(2x-1)$, i.e.,

$$\begin{array}{c|cccccccccc} x & \cdots & -\frac{1}{2} & -\frac{1}{4} & 0 & \frac{1}{4} & \frac{1}{2} & \frac{3}{4} & 1 & \frac{5}{4} & \cdots \\ \hline \varphi(x) & \cdots & 0 & 0 & 1 & 1 & 1 & 1 & 0 & 0 & \cdots \end{array} \quad (7)$$

Eq. (1) reads $\psi(x) = -\varphi(2x-1) + \varphi(2x)$, giving

$$\begin{array}{c|cccccccccc} x & \cdots & -\frac{1}{2} & -\frac{1}{4} & 0 & \frac{1}{4} & \frac{1}{2} & \frac{3}{4} & 1 & \frac{5}{4} & \cdots \\ \hline \psi(x) & \cdots & 0 & 0 & 1 & 1 & -1 & -1 & 0 & 0 & \cdots \end{array} \quad (8)$$

In fact, φ and ψ turn out to be simply the step functions

$$\varphi(x) = \begin{cases} 1 & \text{if } 0 \leq x < 1, \\ 0 & \text{otherwise,} \end{cases} \quad \psi(x) = \begin{cases} 1 & \text{if } 0 \leq x < \frac{1}{2}, \\ -1 & \text{if } \frac{1}{2} \leq x < 1, \\ 0 & \text{otherwise.} \end{cases} \quad (9)$$

□

Example 2.3 (*D4 wavelet*) Let $n=1$, $N=2$ and

$$h_0 = \frac{1+\sqrt{3}}{4\sqrt{2}}, \quad h_1 = \frac{3+\sqrt{3}}{4\sqrt{2}}, \quad h_2 = \frac{3-\sqrt{3}}{4\sqrt{2}}, \quad h_3 = \frac{1-\sqrt{3}}{4\sqrt{2}}. \quad (10)$$

Then the function with the initial values

$$\varphi(1) = \frac{1+\sqrt{3}}{2}, \quad \varphi(2) = \frac{1-\sqrt{3}}{2}, \quad \varphi(k) = 0 \quad \text{for } k \in \mathbb{Z} \setminus \{1, 2\}, \quad (11)$$

²Define, for a given sequence h_0, \dots, h_{2N-1} , the linear operator $T : \mathfrak{F} \rightarrow \mathfrak{F}$ on the function space $\mathfrak{F} = \{f : \mathbb{R} \rightarrow \mathbb{R}\}$ by

$$(Tf)(x) = \sum_{k=0}^{2N-1} h_k f(2x-k).$$

Then the recursion (4) for a function φ means that $\varphi = T\varphi$, i.e., a scaling function is a fixed point of T , i.e., an eigenfunction with eigenvalue 1.

determines the unique scaling function. Eq. (4) then reads $\varphi(x) = \sqrt{2}[h_0 \varphi(2x) + h_1 \varphi(2x - 1) + h_2 \varphi(2x - 2) + h_3 \varphi(2x - 3)]$, i.e.,

x	0	$\frac{1}{4}$	$\frac{1}{2}$	$\frac{3}{4}$	1	$\frac{5}{4}$	$\frac{3}{2}$	$\frac{7}{4}$	2	$\frac{9}{4}$	$\frac{5}{2}$	$\frac{11}{4}$	3
$\varphi(x)$	0	$\frac{5+3\sqrt{3}}{16}$	$\frac{2+\sqrt{3}}{4}$	$\frac{9+5\sqrt{3}}{16}$	$\frac{1+\sqrt{3}}{2}$	$\frac{1+\sqrt{3}}{8}$	0	$\frac{1-\sqrt{3}}{8}$	$\frac{1-\sqrt{3}}{2}$	$\frac{9-5\sqrt{3}}{16}$	$\frac{2-\sqrt{3}}{4}$	$\frac{5-3\sqrt{3}}{16}$	0

(12)

Eq. (1) reads

$$\psi(1) = \sqrt{2}[h_3 \varphi(2) - h_2 \varphi(1) + h_1 \varphi(0) - h_0 \varphi(-1)] = \frac{1 - \sqrt{3}}{2}, \quad (13)$$

and similarly computed for other values,

x	...	0	$\frac{1}{2}$	1	$\frac{3}{2}$	2	$\frac{5}{2}$	3	...
$\psi(x)$...	0	$-\frac{1}{4}$	$\frac{1-\sqrt{3}}{2}$	$\sqrt{3}$	$-\frac{1+\sqrt{3}}{2}$	$-\frac{1}{4}$	0	...

(14)

□

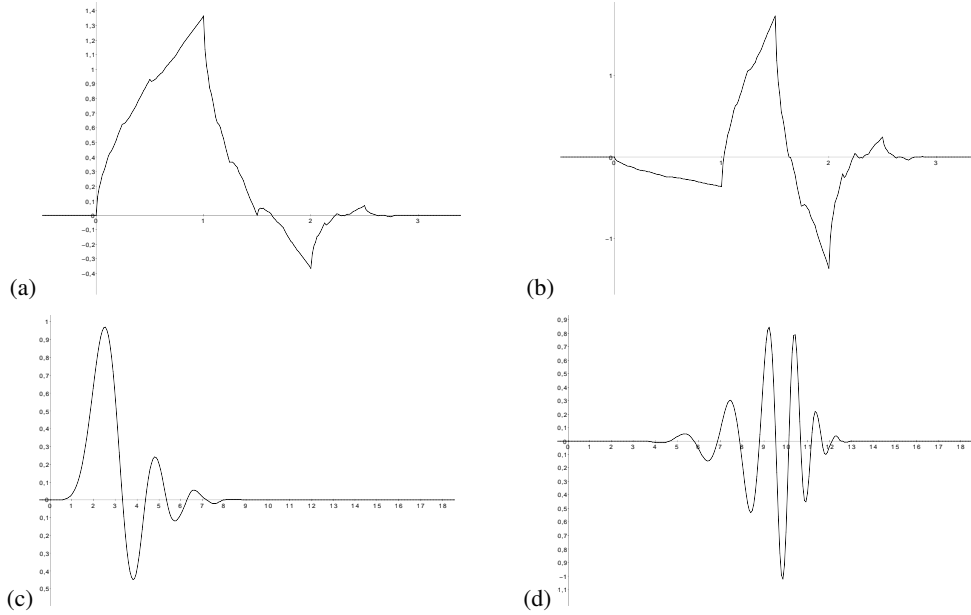


Figure 1: (a) Scaling function ${}_2\varphi$ of Daubechies class D4; (b) wavelet ${}_2\psi$ of Daubechies class D4; (c) scaling function ${}_{10}\varphi$ of Daubechies class D20; (d) wavelet ${}_{10}\psi$ of Daubechies class D20.

Example 2.4 (*Wavelet of Rank 2 and Genus 2*) [10, Ex. 4.3] Let $n = 1$, $N = 2$, and define a one-parameter family of filter coefficients

$$\begin{aligned} h_0(\theta) &= \frac{1 + \sqrt{2} \cos(\theta + \frac{\pi}{4})}{2\sqrt{2}}, & h_0(\theta) &= \frac{1 + \sqrt{2} \cos(\theta - \frac{\pi}{4})}{2\sqrt{2}}, \\ h_1(\theta) &= \frac{1 - \sqrt{2} \cos(\theta + \frac{\pi}{4})}{2\sqrt{2}}, & h_1(\theta) &= \frac{1 - \sqrt{2} \cos(\theta - \frac{\pi}{4})}{2\sqrt{2}}, \end{aligned} \quad (15)$$

where $0 \leq \theta \leq 2\pi$. Especially for $\theta = \frac{\pi}{6}$, these coefficients yield the wavelets of the Daubechies class D4 in Example 2.3. □

Daubechies orthogonal wavelets of classes D2 – D20 (even index numbers only) are the wavelets commonly used. The index number refers to the number $2N$ of coefficients. Each wavelet has a number of vanishing *moments* equal to half the number of coefficients:

$$\int_{\mathbb{R}} x^j {}_N\psi(x) dx = 0 \quad \text{for } j = 0, \dots, N. \quad (16)$$

For example D2 = ψ , the Haar wavelet, has one vanishing moment. D4 = ψ has two moments, etc. A vanishing moment refers to the wavelets ability to represent polynomial behaviour or information in a signal. For example, D2, with one moment, easily encodes polynomials of one coefficient, i.e., constant signal components. D4 encodes polynomials of two coefficients, i.e., constant and linear signal components, D6 encodes 3-polynomials, i.e., constant, linear and quadratic signal components. A high number of vanishing moments for a wavelet leads to a high compressibility since the fine scale wavelet coefficients of a function are essentially zero where the signal function is smooth [3, §7.4].

The regularity of a Daubechies wavelet is measured by the ‘‘Hölder exponent’’ α and proportional to its degree N , viz., $\alpha = \mu_N N$ with a the proportionality factor limited by $\mu_N > 0.2$ [3, §7.1.2]. Especially, $\alpha > 1$ for $N \geq 3$, i.e., ${}_N\phi$, ${}_N\psi$ are continuously differentiable for $N \geq 3$ [3, pp. 226,239]. In general, for fixed support width of ϕ and ψ , or equivalently for a fixed number of non-vanishing filter coefficients h_k , the choice of the h_k which leads to maximum regularity of the wavelet is different from the choice with the maximum number of vanishing moments for the wavelet ψ .

In Table 1, there are listed the coefficients for the scaling functions D2-20. The wavelet coeffi-

D2	D4	D6	D8	D10	D12	D14	D16	D18	D20
0.7071067811865475	0.4829629131445341	0.332670529500825	0.2303778133088964	0.1601023979741929	0.1115407433501095	0.0778520540850037	0.054415842431072	0.0380779473638778	0.0266700579005473
0.7071067811865475	0.8365163037378077	0.8068915093110924	0.748465705529153	0.6038292697971895	0.494623890398433	0.3965393194838912	0.3128715909143166	0.243836746125858	0.188178800776347
	0.2241438680420134	0.4598775021184914	0.6388807679398587	0.7243085284377726	0.7511339080210959	0.7291320908461957	0.6756307462973195	0.6048231246900955	0.5272011889315757
	-0.1294695225512603	-0.1350110200102546	-0.0279837694168599	0.1384281459013203	0.3152503517091982	0.4697822874051889	0.585354683654216	0.6572880780512736	0.6884590394534365
	-0.0854412738820267	-0.1870348117190931	-0.242248870663823	-0.22626469396544	-0.1439060039285212	-0.0158291052563823	0.1331973858249883	0.2811723436605715	
	0.03522629188857095	0.0308413818355607	-0.0322448695846381	-0.129766675672625	-0.2240361849938412	-0.2840155429615824	-0.293273783229492	-0.2498464243271598	
		0.0328830116668852	0.0775714938400459	0.0975016055873225	0.0713092192668272	4.724845739124E-4	-0.0968407832229492	-0.1959462743772862	
			-0.010597401785069	-0.0062414902127983	0.0275228655303053	0.0806126091510774	0.1287474266204893	0.1485407493381256	0.1275693403357541
				-0.012580751999082	-0.0315820393174862	-0.0380299369350104	-0.01736991001809	0.0307256814793305	0.0930878564035547
				0.0033357252834738	5.338422011614E-4	-0.0165745416306655	-0.044882339307971	0.0676328290613279	0.0713941471663301
					0.0047772575109455	0.0125509985560986	0.0139810279174001	2.50947114834E-4	-0.0294575368218399
					-0.0010773010853085	4.295779729214E-4	0.0087460940474065	0.0223616621236798	0.0332126740593612
						-0.0018016407040473	-0.004870352993452	-0.0047232047577518	0.003606553566987
						3.537137999745E-4	-3.91740373377E-4	-0.0042815036824635	-0.0107331754833007
							6.754494064308E-4	0.0018476468830563	0.001395317470688
							-1.174767841248E-4	2.30885763532E-4	0.001992405291925
								-2.19631889427E-4	-6.858566949564E-4
								3.93473203163E-5	-1.16466851285E-4
									9.35886703202E-5
									-1.32642028945E-5

Table 1: Normalized filter coefficients h_k of the orthogonal Daubechies D2N scaling functions ${}_N\phi$, giving the compactly supported wavelets with extremal phase and highest number of vanishing moments compatible with their support width. The values are listed from [3].

cients g_k giving $\psi(x) = \sqrt{2} \sum_k g_k \phi(2x - k)$ are derived from h_k by $g_k = (-1)^k h_{2N+1-k}$, cf (1).

Daubechies [2] proved that the scaling functions ${}_N\phi$, for $N > 1$ are functions which do not admit an algebraic formula in terms of elementary functions. Indeed, they belong to a new class of mathematical functions, different from polynomials or trigonometric, exponential, elliptic, and standard special functions in engineering and physics.

By (4), the Daubechies scaling functions are defined recursively, starting from initial values on the set of integers \mathbb{Z} . The next values to be computed are the values for half-integers $\frac{1}{2}n$, derivable from the initial values. The values computed next are the numbers $\frac{1}{4}n$, then $\frac{1}{8}n$, and so on. Therefore, the function values are usually computed for numbers with finite binary expansion, so-called ‘‘dyadic’’ numbers. However, they are computable for any rational values, e.g., [Abb].³

³Thanks to Paul Abbott for this hint.

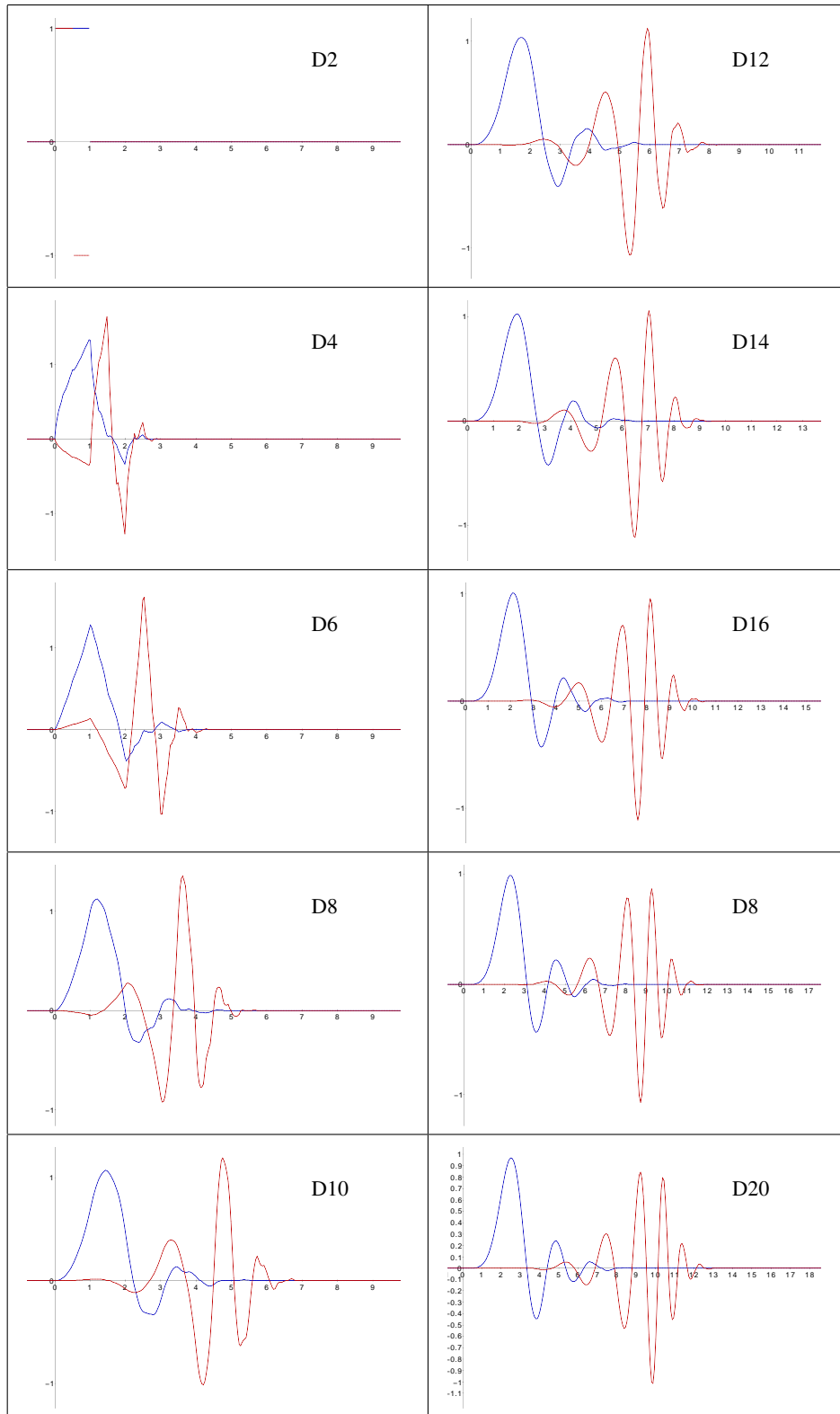


Figure 2: The scaling functions φ_N (blue) and the corresponding wavelets ψ_N (red) of the Daubechiesn class $D(2N)$, for $N = 1, 2, \dots, 10$.

2.1 Dyadic numbers

Definition 2.5 A number $x \in \mathbb{R}$ is called *integer dyadic* if it is an integer multiple of an integer power of 2. The set of all dyadic numbers is denoted by \mathbb{D} , i.e.,

$$\mathbb{D} = \{m \cdot 2^n : m, n \in \mathbb{Z}\}. \quad (17)$$

For an integer $n \in \mathbb{Z}$, a number $x \in \mathbb{R}$ is called *n-dyadic* if it is an integer multiple of 2^{-n} , and the set \mathbb{D}_n denotes the set of all *n-dyadic* numbers,

$$\mathbb{D}_n = \{m \cdot 2^{-n} : m \in \mathbb{Z}\}. \quad (18)$$

□

Generally, $\mathbb{D}_n = 2^{-n}\mathbb{Z}$, especially $\mathbb{D}_0 = \mathbb{Z}$.

Examples 2.6 (a) The number $x = \frac{3}{8}$ is dyadic, since $x = 3 \cdot 2^{-3}$, i.e., $\frac{3}{8} \in \mathbb{D}_3$. It has binary expansion $\frac{3}{8} = 0.011_2$.

(b) The number $x = 4.5$ is dyadic, since $x = 9 \cdot 2^{-1}$, i.e., $4.5 \in \mathbb{D}_1$. It has binary expansion $4.5 = 100.1_2$.

(c) The number $x = \frac{1}{3}$ is *not* dyadic: If integers m and n existed such that $\frac{1}{3} = m/2^n$, we would have $2^n = 3m$, which is impossible since a pure power of 2 cannot be divided by 3 (by the unique prime factorization). It has infinite binary expansion $\frac{1}{3} = 0.0\overline{1}_2$.

(d) Any rational number $\frac{p}{q}$ where $p, q \in \mathbb{Z}$ are relatively prime and where q is no pure power of 2 (i.e., $\nexists n \in \mathbb{Z}$ with $q = 2^n$), is *not* dyadic. Assume that it were dyadic; then there existed $m, n \in \mathbb{Z}$ such that $\frac{p}{q} = m/2^n$, i.e., $q = 2^n p/m \in \mathbb{Z}$; since p and q are relatively prime, p could be canceled at the right hand side, i.e., m would be a multiple of p , but since $2^n p/m$ would be integer, we had $m = 2^k p$ for a $k \leq n$, thus $q = 2^{n-k}$; this would contradict the assumption on q . For instance, $\frac{2}{5} = 0.0\overline{1100}_2$ or $\frac{1}{10} = 0.000\overline{1100}_2$ are not dyadic.

(d) An irrational number $x \in \mathbb{R} \setminus \mathbb{Q}$ is *not* dyadic, since if $m/2^n \in \mathbb{Q}$ for any $m, n \in \mathbb{Z}$. For instance, $x = \sqrt{2} = 2^{1/2}$ is not dyadic. In general, we therefore have the set inclusions

$$\dots \subset \mathbb{D}_{-1} \subset \mathbb{D}_0 \subset \mathbb{D}_1 \subset \dots \subset \mathbb{D}_n \subset \dots \subset \mathbb{D} \subset \mathbb{Q} \subset \mathbb{R}. \quad (19)$$

To summarize, any integer is dyadic, but “most” of the rationals are not, and *a fortiori* any irrational number is not dyadic. Contrary to \mathbb{Q} , the set \mathbb{D} established with the usual multiplication does not form a group (because there does not exist necessarily a multiplicative inverse x^{-1} , e.g., $3 \in \mathbb{D}$ but $\frac{1}{3} \notin \mathbb{D}$), but only a semigroup, just like \mathbb{Z} . □

Definition 2.7 Denote by $\mathbb{D}[\sqrt{3}]$ the set of all linear combinations with dyadic coefficients $p, q \in \mathbb{D}$, i.e.,

$$\mathbb{D}[\sqrt{3}] = \{p + q\sqrt{3} : p, q \in \mathbb{D}\}. \quad (20)$$

Analogously, for $n \in \mathbb{Z}$ denote

$$\mathbb{D}_n[\sqrt{3}] = \{p + q\sqrt{3} : p, q \in \mathbb{D}_n\}. \quad (21)$$

Moreover, for each dyadic number $x \in \mathbb{D}$ define the *conjugate (with respect to $\sqrt{3}$)* by

$$\overline{p + q\sqrt{3}} := p - q\sqrt{3}. \quad (22)$$

□

Example 2.8 For $\frac{9+5\sqrt{3}}{16} = \frac{9}{2^4} + \frac{5}{2^4} \in \mathbb{D}_4[\sqrt{3}]$, we have $\overline{\frac{9+5\sqrt{3}}{16}} = \frac{9-5\sqrt{3}}{16}$. \square

The set $\mathbb{D}[\sqrt{3}]$, established with ordinary addition and multiplication, is an “integral ring”, which means that addition and multiplication obey the laws of commutativity, associativity, and distributivity, both have an additive and a multiplicative neutral element (0 and 1) as well as an additive inverse ($-x$), but not necessarily a multiplicative inverse (x^{-1}), see [8, §3.1].

Theorem 2.9 Let φ be the Daubechies D4 scaling function as defined in Example 2.3. For each dyadic number $r \in \mathbb{D}$ we then have the following properties.

$$\varphi(r) = \mathbb{D}[\sqrt{3}], \quad (23)$$

$$\varphi(r) = \overline{\varphi(3-r)} \quad (24)$$

$$\sum_{k \in \mathbb{Z}} \varphi(r-k) = 1 \quad (25)$$

$$\sum_{k \in \mathbb{Z}} (S_1 + k) \varphi(r-k) = r \quad \text{where } S_1 = \sum_{k=0}^{2N-1} 2kh_{2k} = \frac{3-\sqrt{3}}{2}. \quad (26)$$

Proof. [8, §9.1.2]. \square

Eqs. (23) and (23) show that it suffices to calculate values $\varphi(r)$ only for $0 \leq r \leq \frac{3}{2}$, because the remaining values follow by conjugation. We note that especially for the initial values of φ in (11) we have $\varphi(2) = \overline{\varphi(1)}$. Eq. (25) is called a *partition of unity*, and Eq. (26) is called a *partition of the identity*.

2.2 Properties of Daubechies scaling functions

In this section we will list some general properties about the Daubechies scaling functions which are useful to compute their values, once the filter coefficients h_k are given. First we observe that in general the normalization of the integer initial values also normalize the integral.

Theorem 2.10 For a sequence of filter coefficients h_0, \dots, h_{2N-1} and a continuous function $\varphi \in C^0(\mathbb{R})$ satisfying conditions (2) – (6), together with the additional condition

$$\sum_{n \in \mathbb{Z}} \varphi(n) = 1, \quad (27)$$

then $\int_{\mathbb{R}} \varphi(x) dx = 1$.

Proof. The assertion can be shown by first proving by induction over $m \in \mathbb{N}$ that $\sum_{n \in \mathbb{Z}} \frac{1}{2^m} \varphi\left(\frac{n}{2^m}\right) = 1$, and then approximating the integral by Riemann sums at the midpoints [8, Prop. 9.2]. \square

Next we will consider the initial values for the recursion equation of φ at the “inner integer points” for $N > 1$, where we assume that φ vanishes at the boundaries of the compact support, i.e., $\varphi(0) = \varphi(2N-1) = 0$. (This requirement is due to the assumed continuity of φ and is obsolete for the discontinuous Haar case $N = 1$.) It is directly verified [8, §9.1] that the vector $\mathbf{x} = (\varphi(1), \varphi(2), \dots, \varphi(2N-2))^T$ is an eigenvector with eigenvalue 1 of the $(2N-2) \times (2N-2)$ -matrix $A = (a_{ij})$ with entries

$$a_{ij} = \begin{cases} \sqrt{2}h_{2i-j} & \text{if } 2i-j \in \{0, \dots, 2N-1\}, \\ 0 & \text{otherwise,} \end{cases} \quad (i, j = 1, \dots, 2N-2) \quad (28)$$

i.e., $A\mathbf{x} = \mathbf{x}$. Note that the odd columns of A contain the filter coefficients with odd indices, and the even columns the coefficients with even indices. Together with the additional condition

$$\sum_{n=1}^{2N-2} \varphi(n) = 1 \quad (29)$$

the initial values are unique for $N > 1$ if A is regular (i.e., $\det A \neq 0$).

Example 2.11 Let for $N = 2$ be h_k the coefficients (10) of the Daubechies D4 wavelet. Then

$$A = \sqrt{2} \begin{pmatrix} h_1 & h_0 \\ h_3 & h_2 \end{pmatrix} = \frac{1}{4} \begin{pmatrix} 3 + \sqrt{3} & 1 + \sqrt{3} \\ 1 - \sqrt{3} & 3 - \sqrt{3} \end{pmatrix}. \quad (30)$$

Then $\mathbf{x} = (\varphi(1), \varphi(2))$, and the condition for an eigenvector to the eigenvalue 1 yields the linear equation $(A - I)\mathbf{x} = \mathbf{0}$, or

$$\begin{pmatrix} \sqrt{2}h_1 - 1 & \sqrt{2}h_0 \\ \sqrt{2}h_3 & \sqrt{2}h_2 - 1 \end{pmatrix} \begin{pmatrix} \varphi(1) \\ \varphi(2) \end{pmatrix} = \begin{pmatrix} 0 \\ 0 \end{pmatrix}. \quad (31)$$

The first equation, for instance, yields $\varphi(2) = -\frac{\sqrt{2}h_1 - 1}{\sqrt{2}h_0} \varphi(1) = \frac{1 - \sqrt{3}}{1 + \sqrt{3}} \varphi(1)$, thus $\varphi(1) + \varphi(2) = \frac{2\varphi(1)}{1 + \sqrt{3}}$, and the normalization condition (29) yields the values $\varphi(1)$ and $\varphi(2)$ as in Eq. (11). Since $\det A = 2(h_1h_2 - h_0h_3) = \frac{1}{2}$, the matrix A is regular and the initial values are determined uniquely by the normalization. \square

3 The fast Daubechies wavelet transform

By a linear combination \tilde{f} of shifted scaling functions φ and wavelets ψ , Daubechies wavelets can approximate a function f which may represent an arbitrary signal. The higher the index of the Daubechies wavelets, the smoother the approximation \tilde{f} of f which is known only from an equidistant sample

$$\mathbf{s} = (s_0, s_1, \dots, s_{2^n-2}, s_{2^n-1}).$$

For the fast wavelet transformation to succeed, the sample *must* contain a number of values equal to an integral power of 2, otherwise it becomes necessary to shorten or extend the sample. Here we may assume that the values s sample the signal function f at integer points such that $s_k = f(k)$. (If not, a change of variable $x \rightarrow x/\ell$ allows to consider $s_k = f(k/\ell)$, for the length $\ell > 0$ of the sample interval.) The Daubechies scaling function begins to approximate the sample \mathbf{s} by the linear combination

$$\tilde{f}(x) = \sum_{k=0}^{2^{n+1}-1} a_k^{(n)} \varphi(x - k) \quad (32)$$

with coefficients $a_k^{(n)}$ determined by the signal (s_k) . This is a *discrete convolution* of the signal with the scaling function [9, §13.1]. In essence, the fast Daubechies wavelet transformation consists of two steps in which the signal is convolved with shifted scaling functions and wavelets.

Step 1 (Preprocessing): The first step of the algorithm is to determine the initial values of the coefficients a_0, \dots, a_{2^n-1} . For this purpose, the sample has to be extended by $2^n + N$ entries to

$$\mathbf{s}' = \underbrace{(s_0, s_1, \dots, s_{2^n-2}, s_{2^n-1})}_{\text{sample data}} \underbrace{(s_{2^n}, s_{2^n+1}, \dots, s_{2^{n+1}-2})}_{\text{extension}} \underbrace{(s_0, s_1, \dots, s_{N-1})}_{\text{short extension}}. \quad (33)$$

where N is the number of Daubechies coefficients h_k . Here the values of the extension are computed as

$$s_{2^n} = 2s_0 - s_1, \quad s_k = p(k) \quad \text{for } k = 2^n + 1, \dots, 2^{n+1} - 2, \quad (34)$$

with the cubic spline polynomial

$$p(x) = p_0 + (x + 1 - 2^n) (p_1 + (x - 2^n) (p_2 + p_3 (x + 1 - 2^{n+1}))), \quad (35)$$

given by the coefficients

$$p_0 = s_{2^n-1}, \quad p_1 = s_{2^n-1} - s_{2^n-2}, \quad (36)$$

$$p_2 = \frac{2s_0 - s_1 - s_{2^n-1} - 2^n p_1}{2^n(2^n - 1)}, \quad p_3 = \frac{s_0 - s_{2^n-1} - (2^n + 1)p_1}{2^n(2^n + 1)} - p_2, \quad (37)$$

and the short extension consists of the first N sample values. This yields a ‘‘smooth periodic extension’’ of the original sample.⁴ With the extended sample data array, the coefficients $a_k^{(n)}$ are computed as a weighted average, also called a *convolution*, of the shifted scaling functions:

$$a_k^{(n)} = \sum_{j=k}^{k+2^n-1} s'_j \varphi(j-k) \quad (k = 0, 1, \dots, 2^{n+1} - 1). \quad (38)$$

Step 2 (Recursion): The recursive step of the algorithm is to replace the sum of the scaling functions (32) by a linear combination of half as many coarser scaling functions $\varphi(\frac{x}{2} - 2k)$ and half as many coarser wavelets $\psi(\frac{x}{2} - 2k)$ such that

$$\tilde{f}(x) = \sum_{k=0}^{2^n-1} a_k^{(n-1)} \varphi\left(\frac{x}{2} - 2k\right) + \sum_{k=0}^{2^n-1} c_k^{(n-1)} \psi\left(\frac{x}{2} - 2k\right). \quad (39)$$

The superscripts $(n-1)$ indicate that the frequency of the respective function is lower than the initial $a_k^{(n)}$ -coefficients. The lower coefficients are given by

$$a_k^{(n-1)} = \sum_{j=0}^{N-1} h_j a_{2k+j \bmod 2^{n+1}}^{(n)} \quad (40)$$

$$c_k^{(n-1)} = \sum_{j=0}^{N-1} (-1)^{j+1} h_j a_{2k+2N-1-j \bmod 2^{n+1}}^{(n)} \quad (41)$$

for $k = 0, 1, \dots, 2^{n-1} - 1$. In the next recursion step, the sum of the 2^n scaling functions in (39) is again replaced by a sum of half as many slower scaling functions and wavelets, but the wavelet part

⁴The computation of the smooth periodic extension costs the most running time of the entire algorithm, it has time complexity $T(m) = O(m)$, where $m = 2^n$ is the number of sample values. Since moreover additional values have to be stored, the memory space to store them is doubled. There exist different averaging methods, notably the ‘‘reflection’’ where the extended sample data array is given by

$$s' = \underbrace{(s_0, s_1, \dots, s_{2^n-2}, s_{2^n-1})}_{\text{sample data}} \underbrace{(s_{2^n-1}, s_{2^n-2}, \dots, s_0)}_{\text{reflection}} \underbrace{(s_0, s_1, \dots, s_{N-1})}_{\text{short reflection}}.$$

This efforts no additional computation time or memory space. The disadvantage, however, is a worse approximation of the signal function.

remains unchanged. In this way, the r -th recursion step, with $r = 1, 2, \dots, n+1$, results in the linear combination

$$\tilde{f}(x) = \sum_{l=1}^r \sum_{k=0}^{2^{n-l}-1} c_k^{(n-l)} \psi\left(\frac{x}{2^l} - 2^l k\right) + \sum_{k=0}^{2^{n-r}-1} a_k^{(n-r)} \varphi\left(\frac{x}{2^r} - 2^r k\right) \quad (42)$$

with the coefficients

$$\begin{aligned} a_k^{(n-r)} &= \sum_{j=0}^{N-1} h_j a_{(2k+j) \bmod 2^{n-r+2}}^{(n-r+1)} \\ c_k^{(n-l)} &= \sum_{j=0}^{N-1} (-1)^{j+1} h_j a_{(2k+2N-1-j) \bmod 2^{n-l+2}}^{(n-l+1)} \end{aligned} \quad (43)$$

In this way, each recursion step of the algorithm peels off half of the scaling functions and replaces them by wavelets (Figure 3). After the $(n+1)$ -th recursion, we thus obtain a single scaling function

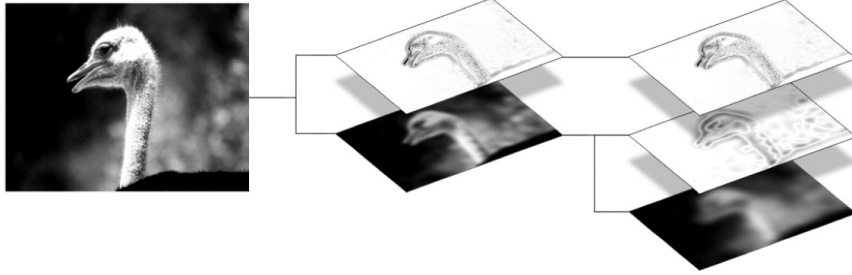


Figure 3: The “peeling-off” of the scaling functions φ and their replacements by wavelets due to the fast wavelet transformation, Eq. (44). This leads to a so-called “multiresolution analysis”, see Definition 4.3 below. The (“low-pass filtered”) wavelet parts remain unchanged by following iterations, whereas the (“high-pass filtered”) scaling function parts is decomposed in the next iteration. Depending on their frequencies, each wavelet part stores coarser information than the foregoing one. Hence the first wavelet represents the finest information of the signal (sharp “edges” for a rough sketch of an image), similarly to the human vision system. Cf. Definition 4.3.

and $n+1$ convolutions of wavelets with different frequencies,

$$\begin{aligned} \tilde{f}(x) &= \sum_{l=1}^{n+1} \sum_{k=0}^{2^{n-l}-1} c_k^{(n-l)} \psi\left(\frac{x}{2^l} - 2^l k\right) + \sum_{k=0}^{2^{n-r}-1} a_k^{(n-r)} \varphi\left(\frac{x}{2^r} - 2^r k\right) \\ &= \sum_{k=0}^{2^{n-1}-1} c_k^{(n-1)} \psi\left(\frac{x}{2} - 2k\right) \\ &\quad \sum_{k=0}^{2^{n-2}-1} c_k^{(n-2)} \psi\left(\frac{x}{4} - 4k\right) \\ &\quad \vdots \\ &\quad + c_0^{(0)} \psi\left(\frac{x}{2^n}\right) + c_1^{(0)} \psi\left(\frac{x}{2^n} - 2^n\right) \\ &\quad + c_0^{(-1)} \psi\left(\frac{x}{2^{n+1}}\right) \\ &\quad + a_0^{(-1)} \varphi\left(\frac{x}{2^{n+1}}\right) \end{aligned} \quad (44)$$

Example 3.1 With $n = 2$ and $N = 2$, consider the sample $s = (0, 1, 2, 3)$. The smooth periodic extension then gives

$$s' = \underbrace{(0, 1, 2, 3)}_{\text{sample}}, \underbrace{(4, 2, 1, -1)}_{\text{extension}}, \underbrace{(0, 1)}_{\text{short ext.}}. \quad (45)$$

This gives $a_0^{(2)} = \sum_0^3 s'_j \varphi(j) = \frac{3-\sqrt{3}}{2}$, $a_1^{(2)} = \sum_1^4 s'_j \varphi(j-1) = \frac{5-\sqrt{3}}{2}$, $a_2^{(2)} = \sum_2^5 s'_j \varphi(j-2) = \frac{7-3\sqrt{3}}{2}$, $a_3^{(2)} = \sum_3^6 s'_j \varphi(j-3) = 3 + \sqrt{3}$, $a_4^{(2)} = \sum_4^7 s'_j \varphi(j-4) = \frac{3+\sqrt{3}}{2}$, $a_5^{(2)} = \sum_5^8 s'_j \varphi(j-5) = \sqrt{3}$, $a_6^{(2)} = \sum_6^9 s'_j \varphi(j-6) = -\frac{1+\sqrt{3}}{2}$, $a_7^{(2)} = \sum_7^{10} s'_j \varphi(j-7) = \frac{1-\sqrt{3}}{2}$. Hence the first recursion step yields

$$(a_0^{(1)}, a_1^{(1)}, a_2^{(1)}, a_3^{(1)}) = \left(\frac{18-5\sqrt{3}}{8}, \frac{7+5\sqrt{3}}{4}, \frac{8+3\sqrt{3}}{8}, 1-5\sqrt{3} \right),$$

$$(c_0^{(1)}, c_1^{(1)}, c_2^{(1)}, c_3^{(1)}) = \left(-\frac{3}{8}, \frac{1-\sqrt{3}}{4}, \frac{1-6\sqrt{3}}{8}, 0 \right).$$

Repeating the foregoing calculations give

$$(a_0^{(0)}, a_1^{(0)}) = \left(\frac{61-21\sqrt{3}}{32}, \frac{35-21\sqrt{3}}{32} \right),$$

$$(c_0^{(0)}, c_1^{(0)}) = \left(\frac{35-11\sqrt{3}}{32}, -\frac{27-3\sqrt{3}}{32} \right),$$

and finally,

$$(a_0^{(-1)}) = \left(\frac{3}{2} \right), \quad (c_0^{(-1)}) = \left(\frac{13+21\sqrt{3}}{32} \right).$$

We thus obtain the wavelet transform

$$\begin{aligned} \tilde{f}(x) = & -\frac{3}{8} \psi\left(\frac{x}{2}\right) + \frac{1-\sqrt{3}}{4} \psi\left(\frac{x}{2}-2\right) + \frac{1-6\sqrt{3}}{8} \psi\left(\frac{x}{2}-4\right) + 0 \cdot \psi\left(\frac{x}{2}-6\right) \\ & + \frac{35-11\sqrt{3}}{32} \psi\left(\frac{x}{4}-4\right) - \frac{27-3\sqrt{3}}{32} \psi\left(\frac{x}{4}-4\right) \\ & + \frac{13+21\sqrt{3}}{32} \psi\left(\frac{x}{8}\right) + \frac{3}{2} \varphi\left(\frac{x}{8}\right) \end{aligned} \quad (46)$$

Cf. [8, Ex. 3.21]. □

3.1 Fast Inverse Daubechies Wavelet Transformation

The Fast Inverse Daubechies Wavelet Transformation starts from a wavelet expansion of the form Eq. (42), or equivalently Eq. (44), and reconstructs the coefficients $a_k^{(n)}$ of Eq. (32) such that the reconstructed function $\tilde{f}(x)$ approximately equals the signal $f(x)$, i.e., $\tilde{f}(x) \approx f(x)$. The algorithm starts with the recursion step labeled $r = n + 1$, i.e., the level $(n - r) = (-1)$, and computes the coefficients $a_k^{(n-r+1)}$ from the coefficients of the foregoing level, $a_k^{(n-r)}$ and $c_k^{(n-r)}$, according to the

following formulas:

$$\begin{aligned}
a_{2k}^{(n-r+1)} &= \sum_{j=0}^{N-1} h_{2j} a_{(k-j) \bmod 2^{n-r+2}}^{(n-r)} + h_{2j+1} c_{(k+j-N+1) \bmod 2^{n-r+2}}^{(n-r)} \\
a_{2k+1}^{(n-r+1)} &= \sum_{j=0}^{N-1} h_{2j+1} a_{(k-j) \bmod 2^{n-r+2}}^{(n-r)} - h_{2j} c_{(k+j-N+1) \bmod 2^{n-r+2}}^{(n-r)}
\end{aligned} \tag{47}$$

Example 3.2 Consider the wavelet expansion from Example 3.1, Eq. (46). In the first step, the coefficients $a_0^{(-1)}$ and $c_0^{(-1)}$ determine the coefficients $a_0^{(0)}$ and $a_1^{(0)}$ via $a_0^{(0)} = h_0 a_0^{(-1)} + h_1 c_0^{(-1)} + h_2 a_0^{(-1)} + h_3 c_0^{(-1)}$ and $a_1^{(0)} = -h_0 c_0^{(-1)} + h_1 a_0^{(-1)} - h_2 c_0^{(-1)} + h_3 a_0^{(-1)}$, i.e.,

$$\left(a_0^{(0)}, a_1^{(0)} \right) = \left(\frac{61 + 21\sqrt{3}}{32}, \frac{35 - 21\sqrt{3}}{32} \right).$$

Repeating this procedure then yields

$$\left(a_0^{(1)}, a_1^{(1)}, a_2^{(1)}, a_3^{(1)} \right) = \left(\frac{18 - 5\sqrt{3}}{8}, \frac{7 + 5\sqrt{3}}{4}, \frac{8 + 3\sqrt{3}}{8}, 1 - \sqrt{3} \right),$$

and then

$$\left(a_0^{(2)}, a_1^{(2)}, \dots, a_7^{(2)} \right) = \left(\frac{3 - \sqrt{3}}{2}, \frac{5 - \sqrt{3}}{2}, \frac{7 - \sqrt{3}}{2}, \frac{3 + \sqrt{3}}{2}, \frac{3 + \sqrt{3}}{2}, \frac{\sqrt{3}}{2}, -\frac{1 + \sqrt{3}}{2}, \frac{1 - \sqrt{3}}{2} \right).$$

Especially for $x = 2$, we thus compute $\tilde{f}(2) = \sum_0^7 a_k^{(2)} \varphi(2 - k) = 2$, i.e., the value $f(2)$ is reproduced exactly. This is the case since f is a linear function. In general, however, \tilde{f} only constitutes an approximation of the signal f . \square

4 General approach to wavelets

To define general wavelets, the Fourier transformation is needed, see Definition 4.2 below. Moreover it is used in wavelet theory to prove basic properties of wavelet. The Fourier transformation is an important integral transformation which is widely used in physics and engineering. A wavelet, being defined in general with the aid of the Fourier transformation, in turn also gives rise to an integral transformation, the wavelet transformation. This way, wavelet transformations are sisters of the Fourier transformation, differing in their integral kernels: the former has a wavelet as integral kernel, whereas the Fourier transformation has an integral kernel consisting of the trigonometric functions (or equivalently, of powers of e^{ix}). While Fourier transformation expands signals (or functions) in terms of infinitely extended sines and cosines (or complex exponentials), wavelet transformations use wavelets, “small waves”, that have their energy concentrated around a point in time or space and usually are finitely extended (“have compact support”).

Therefore wavelet transforms are well localised in time or space in contrast to Fourier transforms which are not localised at all. Because of this property Fourier analysis is very well suited for periodic, time/space-invariant or stationary signals, but naturally not for aperiodic, time/space-varying, transient signals. The two parameter dependency of the wavelet transform makes it superior, since scale and position are varied allowing simultaneous time and frequency analysis. The wavelet transformation is thus similar to a musical score, which tells the musician what note when to play, while the Fourier transformation hides the temporal localisation hidden inaccessibly in the phases.

4.1 The Fourier transformation

Definition 4.1 Let $f \in L^2(\mathbb{R}^n)$. Then its *Fourier transform* $\hat{f} := \mathcal{F}f \in L^2(\mathbb{R}^n)$ is defined as the function

$$\hat{f}(y) = \frac{1}{\sqrt{2\pi^n}} \int_{\mathbb{R}^n} f(x) e^{-iy \cdot x} dx. \quad (48)$$

(Here $y \cdot x = \sum_1^n y_j x_j$ denotes the inner product of the vector space \mathbb{R}^n .) The mapping $\mathcal{F} : L^2(\mathbb{R}^n) \rightarrow L^2(\mathbb{R}^n)$, $f \mapsto \hat{f}$, is called *Fourier transformation*. \square

There is a lot to say about the Fourier transformation, cf. [1]. We restrict ourselves here mentioning that the Fourier transformation \mathcal{F} is a unitary linear mapping $\mathcal{F} : L^2(\mathbb{R}^n) \rightarrow L^2(\mathbb{R}^n)$ on the function space $L^2(\mathbb{R}^n)$, where “unitary” means that \mathcal{F} preserves the length $\|f\| = \sqrt{\langle f, f \rangle}$ of $f \in L^2(\mathbb{R}^n)$. Therefore, the Fourier transformation in fact is just a “coordinate change”, similar to a reflection of basis vectors in \mathbb{R}^n . It satisfies $\mathcal{F}^2 f(x) = f(-x)$ and $\mathcal{F}^4 f(x) = f(x)$, in other words $\mathcal{F}^4 = I$ where I denotes the identity on $L^2(\mathbb{R}^n)$. Hence the Fourier transformation is an “isometry with period 4”. A reflection in \mathbb{R}^n , in comparison, is an “isometry with period 2”, since a reflection applied twice yields the identity.

From the point of view of physics or engineering, the Fourier transformation changes the representation of a function, or “signal”, from the time or space domain into the frequency or wavenumber domain, respectively, and vice versa. Therefore, especially in the theory of signal processing it has invaluable relevance, since with it a signal $f(t)$ in the time domain can be represented as $\hat{f}(\nu)$ in the frequency domain where it may be filtered to a given frequency range.

4.2 Basic properties of wavelets

Definition 4.2 A *wavelet* ψ is a function $\psi \in L^2(\mathbb{R}^n)$ such that its Fourier transform $\hat{\psi} = \mathcal{F}\psi$ satisfies

$$C_\psi := (2\pi)^n \int_{\mathbb{R}} \frac{|\hat{\psi}(tx)|^2}{|t|} dt < \infty \quad (49)$$

for almost all $x \in \mathbb{R}^n$. This condition is often called the *admissibility criterion*. \square

A direct consequence of Eq. (49) is that for a wavelet we always have

$$0 = \hat{\psi}(0) = \int_{\mathbb{R}^n} \psi(x) e^{-2\pi i \cdot 0 \cdot x} dx = \int_{\mathbb{R}^n} \psi(x) dx. \quad (50)$$

Thus, a wavelet has the same volume above the x -axis as below the x -axis. This is where the name wavelet, derived from French *ondelettes* (little waves), has originated.

Definition 4.3 (*Multiresolution analysis*) [6, §4.5] A sequence $\{V_j\}_{j \in \mathbb{Z}}$ of closed subspaces of $L^2(\mathbb{R}^n)$ is a *multiresolution analysis*, or *multiscale analysis*, if the following six properties are satisfied:

$$f(x) \in V_j \Leftrightarrow f(x - 2^j k) \in V_j \quad \forall j \in \mathbb{Z}, k \in \mathbb{Z}^n, \quad (51)$$

$$V_j \subset V_{j-1} \quad \forall j \in \mathbb{Z}, \quad (52)$$

$$f(x) \in V_0 \Leftrightarrow f(2^{-j}x) \in V_j \quad \forall j \in \mathbb{Z}, \quad (53)$$

$$\lim_{j \rightarrow +\infty} V_j = \bigcap_{j=-\infty}^{+\infty} V_j = \{0\}, \quad (54)$$

$$\lim_{j \rightarrow -\infty} V_j = \text{closure} \left(\bigcup_{j=-\infty}^{+\infty} V_j \right) = L^2(\mathbb{R}^n). \quad (55)$$

$$\exists \varphi \in V_0 \text{ such that } \{\varphi(x-k)\}_{k \in \mathbb{Z}^n} \text{ is a Riesz basis of } V_0. \quad (56)$$

A *Riesz basis* $(f_j)_{j \in J}$ of a Hilbert space \mathcal{H} is the image of a Hilbert basis $(e_j)_{j \in J}$ of \mathcal{H} under an isomorphism $A : \mathcal{H} \rightarrow \mathcal{H}$. (Note that A is not necessarily an isometry.) A family $(e_j)_{j \in J}$ of vectors $e_j \in \mathcal{H}$ in a Hilbert space is called *Hilbert basis* if $\text{span}\{e_j : j \in J\}$ is dense in \mathcal{H} , i.e., any vector $x \in \mathcal{H}$ can be approximated arbitrarily close by a linear combination of the vectors e_j . The function φ is called *scaling function* or *father wavelet*. \square

With a Riesz basis, a vector $x \in \mathcal{H}$ is therefore uniquely decomposed in a series

$$x = \sum_{j \in J} \alpha_j f_j, \quad \text{where } \sum_{j \in J} |\alpha_j|^2 < \infty. \quad (57)$$

Furthermore, $\langle x, f_j^* \rangle$ where $f_j^* = (A^*)^{-1} e_j$ is the dual basis of f_j , being itself a Riesz basis. The two systems (f_j) and (f_j^*) are said to be *biorthogonal*. Hence multiresolution analysis leads to the concept of orthonormal wavelets, as well as of biorthogonal wavelets, as we will see below.

Condition (53) is the essential requirement implying multiresolution as the increment in information by going from a fine scale approximation (j) to a coarser resolution approximation ($j+1$). Here

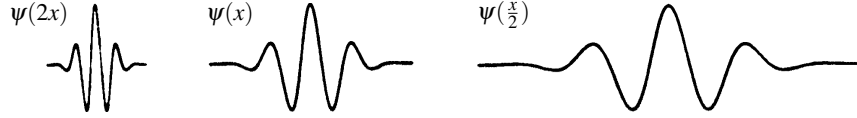


Figure 4: Dilations of a wavelet $\psi(x) \in V_0$. If condition (53) is satisfied, then $\psi(2x) \in V_{-1}$ and $\psi(\frac{x}{2}) \in V_1$. In a multiresolution analysis, $V_{-1} \supset V_0 \supset V_1$.

the factor 2^j is the *dilation* which stretches the function f with respect to the level $j=0$ (Figure 4). Condition (51) implies another feature of multiresolution analysis, i.e., invariance of V_0 under integer translations, $f(x) \in V_0 \Leftrightarrow f(x-k) \in V_0$. Finally, condition (56) guarantees that for each $j \in \mathbb{Z}$, the functions

$$\varphi_{jk}(x) = 2^{-j/2} \varphi(2^{-j}x - k) \quad (k \in \mathbb{Z}^n) \quad (58)$$

form a Riesz basis for V_j . In particular, if $\varphi_{0k}(x) = \varphi(x-k)$ is an orthonormal basis of V_0 , then φ_{jk} is an orthonormal basis of V_j [3, §5.1].

In the language of multiresolution analysis, V_j is thus the closed subspace of $L^2(\mathbb{R}^n)$ spanned by the basis $2^{-j/2} \varphi(2^{-j}x - k)$, $k \in \mathbb{Z}^n$. Analogously, the orthogonal complement W_j of V_j in V_{j-1} , that means

$$V_j \oplus W_j = V_{j-1}, \quad (59)$$

has a Riesz basis $2^{-j/2} \psi(2^{-j}x - k)$, $k \in \mathbb{Z}^n$. In this light, the constructions of the wavelets packets we will consider later on appears as a change of basis inside each W_j . We have $W_j \perp W_l$ if $j \neq l$, and it follows

$$V_j = V_m \oplus \bigoplus_{l=0}^{m-j-1} W_{m-l} \quad \text{for } j < m. \quad (60)$$

By (54) and (55) this implies $L^2(\mathbb{R}^n) = \bigoplus_{j \in \mathbb{Z}} W_j$. Thus, a multiresolution analysis yields a decomposition of $L^2(\mathbb{R}^n)$ into mutually orthogonal subspaces. The spaces W_j inherit the scaling property (53) from the spaces V_j , i.e.,

$$f(x) \in W_j \Leftrightarrow f(2^j x) \in W_0. \quad (61)$$

Therefore, once a wavelet ψ is known such that $\psi_{0,k} = \psi(x-k)$ with $k \in \mathbb{Z}^n$ forms a Riesz basis, or even an orthonormal basis, of W_0 , then for each $j \in \mathbb{Z}$ the functions $\psi_{j,k} = 2^{-j/2}\psi(2^{-j}x-k)$ with $k \in \mathbb{Z}^n$ form a Riesz basis or an orthonormal basis, respectively, of W_j , and $(\psi_{j,k})$ with $k \in \mathbb{Z}^n$, $j \in \mathbb{Z}$ forms a respective basis of $L^2(\mathbb{R}^n)$. Such a wavelet ψ can be constructed from the scaling function φ by simple procedure using the following properties of φ and W_0 .

Since $\varphi \in V_0 \subset V_{-1}$ and the $\varphi_{-1,k}$ form a basis in V_{-1} , we have $\varphi = \sum_{k \in \mathbb{Z}^n} h_k \varphi_{-1,k}$ where the constants $h_k \in \mathbb{C}$ are determined by

$$h_k = \langle \varphi, \varphi_{-1,k} \rangle \quad \text{for } k \in \mathbb{Z}^n. \quad (62)$$

Then we can write either

$$\varphi(x) = \sqrt{2} \sum_{k \in \mathbb{Z}^n} h_k \varphi(2x-k), \quad \text{or} \quad \mathcal{F}\varphi(y) = \frac{1}{2} \sum_{k \in \mathbb{Z}^n} h_k e^{-iky/2} \mathcal{F}\varphi\left(\frac{y}{2}\right), \quad (63)$$

where convergence in the series holds in L^2 -sense. The last formula can be rewritten as

$$\mathcal{F}\varphi(y) = m_0\left(\frac{y}{2}\right) \mathcal{F}\varphi\left(\frac{y}{2}\right), \quad \text{where} \quad m_0(y) = \frac{1}{2} \sum_{k \in \mathbb{Z}^n} h_k e^{-iky/2}. \quad (64)$$

In case that φ provides an orthonormal basis, we have $\sum_k |h_k|^2 = 1$, and m_0 is a 2π -periodic function, and [3, Eq. (5.1.20)]

$$|m_0(y)|^2 + |m_0(y+\pi)|^2 = 1 \text{ a.e.} \quad (65)$$

For the one-dimensional case $n = 1$ and for a finite number N of coefficients h_k it can be proved [3, Theorem 5.1.1] that for a multiresolution analysis a wavelet ψ can be constructed from φ by the formula

$$\mathcal{F}\psi(y) = e^{-iy/2} \bar{m}_0\left(\frac{y}{2} + \pi\right) \mathcal{F}\varphi\left(\frac{y}{2}\right) \quad (66)$$

or equivalently

$$\psi(x) = \sqrt{2} \sum_k (-1)^{k-1} h_{2N-k-1} \varphi(2x-k) \quad (67)$$

The wavelet ψ is unique up to a phase change and a shift by an integer.

4.2.1 Wavelets and subband filters

Multiresolution analysis in dimension $n = 1$ leads naturally to a hierarchical and fast scheme for the wavelet coefficients of a given function. Suppose that we have computed, or given, the inner products of a signal f with the wavelets φ_{jk} at some given fine scale. By rescaling either our units or the function f we may assume that the label of this fine scale is $j = 0$. Eq. (67) can be rewritten as

$$\psi = \sum_k g_k \varphi_{-1,k} \quad (68)$$

where $g_k = \langle \psi, \varphi_{-1,k} \rangle = (-1)^k h_{2N-1-k}$ [3, Eq. (5.1.35)]. Consequently,

$$\psi_{jk} = 2^{-j/2} \psi(2^{-j}x-k) = 2^{-j/2} \sum_l g_l 2^{1/2} \varphi(2^{-j+1}x-2k-l) = \sum_l g_l \varphi_{j-1,2k+l}(x) = \sum_l g_{l-2k} \varphi_{j-1,l}(x),$$

hence $\langle f, \psi_{1,k} \rangle = \sum_l \bar{g}_{l-2k} \langle f, \varphi_{0,l} \rangle$, i.e., $\langle f, \psi_{1,k} \rangle$ is a convolution of the sequence $(\langle f, \varphi_{0,l} \rangle)_{l \in \mathbb{Z}}$ with $(\bar{g}_{-l})_{l \in \mathbb{Z}}$, retaining only the even samples. Similarly,

$$\langle f, \psi_{j,k} \rangle = \sum_l \bar{g}_{l-2k} \langle f, \varphi_{j-1,l} \rangle. \quad (69)$$

Therefore, also $\langle f, \psi_{j,k} \rangle$ are given by the convolution with \bar{g}_l and decimation (“*subsampling*”) by factor 2 with the $\langle f, \varphi_{j-1,k} \rangle$, which are given by $\langle f, \varphi_{j,k} \rangle = \sum_l \bar{h}_{l-2k} \langle f, \varphi_{j-1,l} \rangle$, cf. [3, Eq. (5.6.4)], since $\varphi_{jk} = 2^{-j/2} \varphi(2^{-j}x - k) = \sum_l h_{l-2k} \varphi_{j-1,l}(x)$. Thus the procedure is simply to start from $\langle f, \varphi_{0,k} \rangle$ and compute recursively $\langle f, \psi_{j,k} \rangle$ and $\langle f, \varphi_{j,k} \rangle$ from the respective $(j-1)$ -value.

The whole process can also be viewed as the computation of successively coarser approximations of f , together with the difference in information between successive j -levels. From this point of view, we start with a fine scale approximation $f^{(0)} = \mathbb{P}_{V_0} f$, where \mathbb{P}_{V_0} denotes the orthogonal projection onto the subspace V_0 , and in each recursion step we decompose $f^{(j-1)} \in V_{j-1} = V_j \oplus W_j$ into $f^{(j-1)} = f^{(j)} + q^{(j)}$, where $f^{(j)} = \mathbb{P}_{V_j} f^{(j-1)}$ is the projection onto V_j , i.e., the next coarser approximation step in the multiresolution analysis, and $q^{(j)} = f^{(j-1)} - f^{(j)} = \mathbb{P}_{W_j} f = \mathbb{P}_{W_j} f^{(j-1)}$ is the information “lost” in the transition $f^{(j-1)} \rightarrow f^{(j)}$. Since in the spaces V_j and W_j we have the Riesz bases (φ_{jk}) and (ψ_{jk}) , respectively, we have

$$f^{(j)} = \sum_k a_k^{(j)} \varphi_{jk}, \quad q^{(j)} = \sum_k c_k^{(j)} \psi_{jk} \quad (70)$$

for some constants $a_k^{(j)}$ and $c_k^{(j)}$. We thus see that in each recursion step,

$$a_l^{(j)} = \sum_k \bar{h}_{l-2k} a_k^{(j-1)} \quad c_l^{(j)} = \sum_k \bar{g}_{l-2k} a_k^{(j-1)}. \quad (71)$$

The inverse transformation yields analogously [3, Eq. (5.6.6)]

$$a_l^{(j-1)} = \sum_k h_{l-2k} a_k^{(j)} + g_{l-2k} c_k^{(j)}. \quad (72)$$

In electrical engineering, the formulas (71) and (72) express the analysis and synthesis steps of a *subband filtering scheme* with exact reconstruction. In a two-channel subband filtering scheme, an incoming sequence $(a_k^{(0)})$ is convolved with two different filters, a low-pass and a high-pass filter. The two resulting sequences are then “subsampled”, i.e., only the even or only the odd (depending on

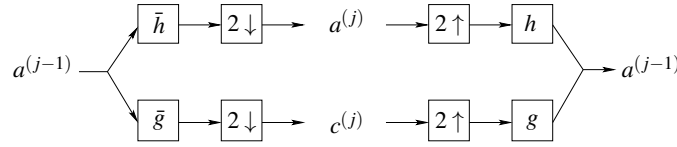


Figure 5: Subband filtering scheme for an analysis and a synthesis step in multiresolution analysis. The steps are given in (71) and (72).

the value n in (72)) entries are retained.

Example 4.4 (*Cubic spline scaling function*) Define φ by its Fourier transform

$$\mathcal{F} \varphi(y) = \frac{1}{\sqrt{2\pi}} e^{-2iy} \left(\frac{e^{iy} - 1}{iy} \right)^4 = \frac{1}{\sqrt{2\pi}} \left(\frac{\sin y/2}{y/2} \right)^4, \quad (73)$$

and the corresponding wavelet by

$$\psi(x) = C_0 \left(-\frac{1}{2} \varphi(x+1) + \varphi(x) - \frac{1}{2} \varphi(x-1) \right) \quad (74)$$

with $C_0 = 6\sqrt{\frac{70}{1313}}$. Then φ is the basic *cubic spline*

$$\varphi(x) = \begin{cases} \frac{1}{6}(2-|x|)^3 & \text{if } 1 \leq |x| < 2, \\ \frac{2}{3} - x^2(1-|x|/2) & \text{if } |x| \leq 1, \\ 0 & \text{otherwise.} \end{cases} \quad (75)$$

This can be seen by noticing that φ is the convolution of the triangle function T with itself, i.e., $\varphi = T * T$, where $T = 1 - |x|$ if $|x| \leq 1$ and $T(x) = 0$ if $|x| > 1$, and that $\mathcal{F}\varphi = (\mathcal{F}T)^2$. The scaling function φ and the wavelet ψ look similar to the Gaussian and its second derivative, the ‘‘Mexican hat’’, respectively. Note, however, that neither the Gaussian, nor its second derivative have compact support, whereas ϕ and ψ are compactly supported. The wavelet ψ clearly satisfies (68) with $g_0 = C_0$, $g_{\pm 1} = -C_0/2$, $g_k = 0$ for $k \neq 0, \pm 1$, whereas $\mathcal{F}\varphi(2y) = (\cos y/2)^4 \mathcal{F}\varphi(y)$, such that Eq. (63) becomes $\varphi(x) = \sum_k h_k \varphi(2x - k)$, with $h_0 = \frac{3}{4}$, $h_{\pm 1} = \frac{1}{2}$, $h_{\pm 2} = \frac{1}{8}$, and $h_k = 0$ for $k \neq 0, \pm 1, \pm 2$. The scaling functions $\varphi_{j,k}$, given by $\varphi_{j,k}(x) = 2^{-j/2} \varphi(2^{-j}x - k)$, do not form a basis of $L^2(\mathbb{R})$, but only a ‘‘frame’’, i.e., there exist constants $0 < A \leq B < \infty$ such that for all $f \in L^2(\mathbb{R})$ we have

$$A\|f\|^2 \leq \sum_{j,k} |\langle f, \varphi_{j,k} \rangle|^2 \leq B\|f\|^2,$$

where here $A = .73178$ and $B = 1.77107$ [3, §3.3.5.D]. \square

4.3 Orthonormal wavelet packets

According to the procedure outlined in [6, §7.2], for a given $N \in \mathbb{N}$ we will construct a sequence of functions w_l , $l \in \mathbb{N}_0$ which vanish outside the hypercube $[0, 2N - 1]^n$ and which bear the property that the $(n + 1)$ -fold sequence $w_l(x - k)$ with $l \in \mathbb{N}_0$ and $k \in \mathbb{Z}^n$ is an orthonormal basis of $L^2(\mathbb{R}^n)$. These functions w_l are called ‘‘wavelet packets’’.

Let be $n, N \geq 1$, and define $\mathbb{Z}_{2N}^n = \{0, 1, \dots, 2N - 1\}^n$ as the n -dimensional grid of $(2N)^n$ discrete grid points. Thus, $k \in \mathbb{Z}_{2N}^n$ is a multi-index $k = (k_1, \dots, k_n)$ with $k_j \in \{0, 1, \dots, 2N - 1\}$. Especially for $n = 1$, we have simply $\mathbb{Z}_{2N}^1 = \{0, 1, \dots, 2N - 1\}$. Consider then constants $h_k \in \mathbb{C}$, where $k \in \mathbb{Z}_{2N}^n$, such that the trigonometric sum $m_0 : \mathbb{R}^n \rightarrow \mathbb{C}$,

$$m_0(y) = \frac{1}{2^n} \sum_{k \in \mathbb{Z}_{2N}^n} h_k e^{-iky}, \quad (76)$$

(where $ky = \sum_j k_j y_j$) satisfies the conditions

$$m_0(0) = 1, \quad m_0(y) \neq 0 \text{ for } y \in [-\frac{\pi}{2}, \frac{\pi}{2}]^n, \quad \sum_{k \in \mathbb{Z}_2^n} m_0(y + \pi k) = 1, \quad (77)$$

where $\mathbb{Z}_2^n = \{0, 1\}^n$ denotes the n -dimensional grid of the 2^n grid points $(0, \dots, 0, 0)$, $(0, \dots, 1, 0)$, \dots , $(1, \dots, 1, 1)$, in other words the corners of the unit n -dimensional hypercube. The function m_0 is the ‘‘minimum phase filter’’ and is directly related to a ‘‘quadrature mirror filter’’ or ‘‘FIR (finite impulse response)’’, and the coefficients h_k correspond to its ‘‘impulse responses’’. Having selected the coefficients h_k , we define the *wavelet packets* w_l by induction on $l = 0, 1, 2, \dots$, using the two identities

$$w_{2l}(x) = \sum_{k \in \mathbb{Z}_{2N}^n} h_k w_l(2x - k), \quad (78)$$

$$w_{2l}(x) = \sum_{k \in \mathbb{Z}_{2N}^n} (-1)^{|k|+1} \bar{h}_{k_* - k} w_l(2x - k), \quad (79)$$

where $k_* = (2N - 1, \dots, 2N - 1) \in \mathbb{Z}_{2N}^n$, and where $w_0 = \varphi$ is defined by its Fourier transform

$$\mathcal{F} \varphi(y) = \prod_{j=0}^{\infty} m_0(2^{-j}y). \quad (80)$$

The infinite product on the right hand side indeed converges absolutely and uniformly on compact sets, since by $\sum_n |h_k| |k| < \infty$ and $m_0(0) = 1$ we have $|m_0(y)| \leq 1 + |m_0(y) - 1| \leq 1 + \sum_k |h_k| |\sin \frac{ky}{2}| \leq 1 + C|y| \leq e^{C|y|}$. On the other hand, the function φ can be constructed iteratively. It is called the *scaling function* or *father wavelet*. Once it is constructed, it can be used by Eq. (79) to obtain the *mother wavelet* $\psi = w_1$. By repeating this process, we generate, two at a time, all wavelet packets. The support of all w_l is included in $[0, 2N - 1]^n$. The central result about the basic wavelet packets is that the $(n + 1)$ -fold sequence $w_l(x - k)$ with $l \in \mathbb{N}_0$, $k \in \mathbb{Z}^n$, is an orthonormal basis for $L^2(\mathbb{R}^n)$. To be more precise, the subsequence $\{w_l\}$ by taking $2^j \leq l \leq 2^{j+1}$ is an orthonormal basis of the orthogonal complement W_j of V_j in V_{j+1} .

Example 4.5 (Daubechies wavelets) For $n = 1$, we chose the nonnegative trigonometric sum

$$P_N(y) = 1 - \frac{1}{c_N} \int_0^y (\sin u)^{2N-1} du \quad (81)$$

with the constant $c_N = \int_0^\pi (\sin u)^{2N-1} du$ such that $P_N(\pi) = 0$. Then by a classical result known as the Fejér-Riesz lemma, there exists a finite trigonometric sum $m_0(y) = \frac{1}{2} \sum_0^{2N-1} h_k e^{-iky}$ with real h_k such that $|m_0(y)|^2 = P_N(y)$ and $m_0(0) = 1$. For $N = 1$, for instance, we have $h_0 = h_1 = 1$, hence $m_0 = \frac{1}{2}(1 + e^{-iy})$, and the last condition in (77) reduces to $\cos^2 \frac{y}{2} + \sin^2 \frac{y}{2} = 1$; this is the Haar wavelet. For $N = 2$, on the other hand, we achieve for h_0, \dots, h_3 given by (10) the Daubechies D4 scaling function φ and the corresponding wavelet ψ is given by $\psi = w_1$. See [3, §6], [6, §§3.8 & 7.2]. \square

4.4 Biorthogonal wavelets

From a practical point of view, signal processing always has to deal with the quantization problem. As long as we stay in a L^2 setting, any orthonormal basis allows a signal to be reconstructed exactly. In practice, however, the coefficients of a signal decomposition must be quantized. Such approximations arise from a limited machinery accuracy or are imposed by a desire to compress the data. If we use a discontinuous wavelet, such as the Haar wavelet, it happens that spurious edges appear and the visual effects can be annoying.

Although the use of smooth orthogonal wavelets produce better results, they have not completely satisfied the experts in image processing. One reason is the lack of symmetry. The scaling function φ should be even, i.e., $\varphi(x) = \varphi(-x)$, and the wavelet ψ should be symmetric around $x = \frac{1}{2}$, i.e.,

$$\psi(1 - x) = \psi(x). \quad (82)$$

A lack of this symmetry in combination with quantization leads to visible defects. The reason is that quantization errors usually are most prominent around edges in images, and our visual system seems to be more tolerant of symmetric errors than of asymmetric ones. Moreover, symmetric filters make it easier to deal with the boundaries of an image. Symmetric filters are also called “linear phase filters” by engineers, which more precisely means that the function $h(y) = \sum_k h_k e^{-iky}$ of a filter with filter coefficients h_k satisfies $h(y) = e^{-ily} |h(y)|$ for some half-integer l , which is equivalent $h_k = h_{2l-k}$.

Although certain orthogonal wavelets in fact are symmetric, they do not hold for wavelets with compact support. The Haar system, being both antisymmetric about $x = \frac{1}{2}$ and compactly supported,

is the only exception to this rule [3, Theorem 8.1.4], but it is not continuous. However, giving up the condition of orthogonality, we gain a degree of freedom which enables us to incorporate the desired symmetries together with continuity and compact support property. This leads us to biorthogonal wavelets, which are implemented in the JPEG-2000 image format.

To introduce biorthogonal wavelets, we first consider the basic one-dimensional case which is later used to construct two-dimensional biorthogonal wavelets.

4.4.1 The one-dimensional case

Instead of an orthonormal basis derived from a single wavelet, we weaken the definition and use two wavelet functions ψ and $\tilde{\psi}$ which will determine two nonorthogonal Riesz bases

$$\psi_{jk} = 2^{j/2} \psi(2^j - k) \quad \text{and} \quad \tilde{\psi}_{jk} = 2^{j/2} \tilde{\psi}(2^j - k), \quad (83)$$

$j, k \in \mathbb{Z}$, each dual to each other. The first basis will be used for synthesis, the second for analysis. This weakening of the definition of a wavelet basis and the flexibility by not requiring, as in the case of orthogonal wavelets, the equality $\psi = \tilde{\psi}$ allows us to make considerable stronger demands on ψ , for instance the requirement (82). To construct the wavelets ψ and $\tilde{\psi}$, we first seek the values of *two* families of “filter coefficients” h_k, \tilde{h}_k having to satisfy

$$\sum_k h_k \tilde{h}_{k+2l} = \delta_{0,l}, \quad \left(\sum_k h_k \right) \left(\sum_k \tilde{h}_k \right) = 2, \quad (84)$$

and determining the scaling functions $\tilde{\varphi}$ and $\tilde{\psi}$ via

$$m_0(y) = \frac{1}{\sqrt{2}} \sum_k h_k e^{iky}, \quad \tilde{m}_0(y) = \frac{1}{\sqrt{2}} \sum_k \tilde{h}_k e^{iky} \quad (85)$$

and

$$\mathcal{F} \varphi(y) = \frac{1}{\sqrt{2\pi^n}} \prod_{j=1}^{\infty} m_0(2^{-j}y), \quad \mathcal{F} \tilde{\varphi}(y) = \frac{1}{\sqrt{2\pi^n}} \prod_{j=1}^{\infty} \tilde{m}_0(2^{-j}y), \quad (86)$$

cf. [3, §8.3.2]. The same argument as used after Eq. (80) proves that both infinite products converge absolutely and uniformly. Then the wavelets ψ and $\tilde{\psi}$ are defined by its Fourier transforms

$$\mathcal{F} \psi(y) = m_1\left(\frac{y}{2}\right) \mathcal{F} \varphi\left(\frac{y}{2}\right), \quad \mathcal{F} \tilde{\psi}(y) = \tilde{m}_1\left(\frac{y}{2}\right) \mathcal{F} \tilde{\varphi}\left(\frac{y}{2}\right), \quad (87)$$

with the functions $m_1(y) = \tilde{m}_0^*(y + \pi) e^{-iy}$, $\tilde{m}_1(y) = \tilde{m}_0^*((y + \pi) e^{-iy})$. (The superscript * denotes complex conjugation.)

Therefore, the general procedure is to suppose two trigonometric sums m_0 and \tilde{m}_0 , the “minimum phase filters” or “low-pass filters”, and to *derive* from them the filter coefficients h_k and \tilde{h}_k and the wavelets. The great advantage now is that we then can impose desired symmetry properties on m_0 and \tilde{m}_0 . Let denote N and \tilde{N} the number of of “taps”, i.e., half of the number of nonvanishing filter coefficients h_k and \tilde{h}_k , respectively. Then if the filters corresponding to m_0 and \tilde{m}_0 , respectively, have both odd numbers N and \tilde{N} of taps, the trigonometric sums m_0 and \tilde{m}_0 can be written as

$$m_0(y) = e^{-iny} p_0(\cos y), \quad \tilde{m}_0(y) = e^{-iny} \tilde{p}_0(\cos y) \quad (N, \tilde{N} \text{ odd}), \quad (88)$$

for two polynomials p_0 and \tilde{p}_0 satisfying

$$p_0(x) \tilde{p}_0^*(x) + p_0(-x) \tilde{p}_0^*(-x) = 1 \quad (N, \tilde{N} \text{ odd}). \quad (89)$$

This equation is the Bezout problem which is solved in essence by applying Euclid's algorithm applied to polynomials being relatively prime [3, Theorem 6.1.1]. For even numbers N and \tilde{N} of taps, we use the ansatz

$$m_0(y) = e^{-i(n-1/2)y} \cos \frac{y}{2} p_0(\cos y), \quad \tilde{m}_0(y) = e^{-iy} \cos \frac{y}{2} \tilde{p}_0(\cos y) \quad (N, \tilde{N} \text{ even}), \quad (90)$$

for two polynomials p_0 and \tilde{p}_0 being related such that \tilde{p}_0 solves the Bezout problem

$$p_0^\#(x) \tilde{p}_0^*(x) + p_0^\#(-x) \tilde{p}_0^*(-x) = 1 \quad (N, \tilde{N} \text{ even}), \quad (91)$$

where $p_0^\#(x) = \frac{1+x}{2} p_0(x)$.

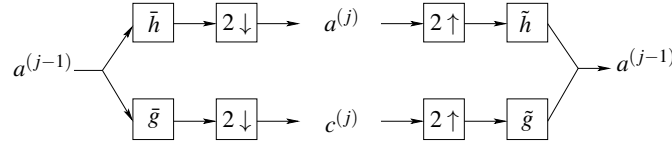


Figure 6: Subband filtering scheme with exact synthesis for an analysis and a synthesis step in multiresolution analysis, but with analysis filters (\tilde{h}_k and \tilde{g}_k) different from the synthesis filters (\tilde{h}_k and \tilde{g}_k).

Example 4.6 (*Daubechies* (\tilde{N}, N) wavelets) Set $n = 0$ and $\tilde{p}_0(x) = x^{\tilde{N}}$. Then either $N = 2l$ and $\tilde{N} = 2\tilde{l}$, and we have

$$\tilde{m}_0(y) = \left(\cos \frac{y}{2}\right)^{2\tilde{l}}, \quad m_0(y) = \left(\cos \frac{y}{2}\right)^{2l} \sum_{m=0}^{l+\tilde{l}-1} \binom{l+\tilde{l}-1+m}{m} \left(\sin \frac{y}{2}\right)^{2m}, \quad (92)$$

or $N = 2l + 1$ and $\tilde{N} = 2\tilde{l} + 1$, and we have

$$\tilde{m}_0(y) = \left(\cos \frac{y}{2}\right)^{2\tilde{l}+1}, \quad m_0(y) = e^{-iy} \left(\cos \frac{y}{2}\right)^{2l+1} \sum_{m=0}^{l+\tilde{l}} \binom{l+\tilde{l}+m}{m} \left(\sin \frac{y}{2}\right)^{2m}, \quad (93)$$

see [3, §8.3.4]. In both cases we can choose $l \in \mathbb{N}$ freely. The result is a family of biorthogonal bases in which $\tilde{\psi}$ is a spline function of compact support. For each preassigned order \tilde{l} of this spline function, there exists an infinity of choices for l , corresponding to different wavelets ψ with increasing support widths, and different wavelets $\tilde{\psi}$ with increasing number of vanishing moments. Note that the scaling function $\tilde{\phi}$ is completely fixed by \tilde{N} alone, while m_0 and hence ϕ depends on both N and \tilde{N} . Hence we denote them by $_{\tilde{N}}\tilde{\phi}$ and $_{\tilde{N}, N}\tilde{\psi}$, $_{\tilde{N}, N}\phi$, and $_{\tilde{N}, N}\psi$. Some concrete values of the filter coefficients h_k are listed in Table 2. The resulting scaling function $_{\tilde{N}}\tilde{\phi}$ is a basic spline of order $(\tilde{N} - 1)$, e.g., the piecewise constant and piecewise linear spline,

$${}_1\tilde{\phi}(x) = \begin{cases} 1 & \text{if } 0 \leq x \leq 1, \\ 0 & \text{otherwise,} \end{cases} \quad {}_2\tilde{\phi}(x) = \begin{cases} 1 - |x| & \text{if } |x| \leq 1, \\ 0 & \text{otherwise,} \end{cases} \quad (94)$$

respectively, as well as the piecewise quadratic spline

$${}_3\tilde{\phi}(x) = \begin{cases} \frac{1}{2}(x+1)^2 & \text{if } -1 \leq x < 0, \\ \frac{3}{4} - (x - \frac{1}{2})^2 & \text{if } 0 \leq x < 1, \\ \frac{1}{2}(x-2)^2 & \text{if } 1 \leq x < 2, \\ 0 & \text{otherwise,} \end{cases} \quad (95)$$

[3, §5.4]. □

$\tilde{N} = 2$	k	\tilde{h}_k	h_k
$N = 2$	0	$\frac{1}{2}$	$+\frac{3}{4}$
	± 1	$\frac{1}{4}$	$+\frac{1}{4}$
	± 2		$-\frac{1}{8}$
$N = 8$	0	$\frac{1}{2}$	$+\frac{22050}{2^{15}}$
	± 1	$\frac{1}{4}$	$+\frac{10718}{2^{15}}$
	± 2		$-\frac{3796}{2^{15}}$
	± 3		$-\frac{3126}{2^{15}}$
	± 4		$+\frac{1228}{2^{15}}$
	± 5		$+\frac{670}{2^{15}}$
	± 6		$-\frac{300}{2^{15}}$
	± 7		$-\frac{70}{2^{15}}$
	± 8		$+\frac{35}{2^{15}}$

$\tilde{N} = 3$	k	$\tilde{h}_k = \tilde{h}_{1-k}$	$h_k = h_{1-k}$
$N = 3$	1	$\frac{3}{8}$	$+\frac{45}{64}$
	2	$\frac{1}{8}$	$-\frac{7}{64}$
	3		$-\frac{9}{64}$
	4		$+\frac{3}{64}$
$N = 9$	1	$\frac{3}{8}$	$\frac{87318}{2^{17}}$
	2	$\frac{1}{8}$	$+\frac{190}{2^{17}}$
	3		$-\frac{29676}{2^{17}}$
	4		$+\frac{1140}{2^{17}}$
	5		$+\frac{9188}{2^{17}}$
	6		$-\frac{1308}{2^{17}}$
	7		$-\frac{1911}{2^{17}}$
	8		$+\frac{469}{2^{17}}$
	9		$+\frac{189}{2^{17}}$
	10		$-\frac{63}{2^{17}}$

Table 2: Filter bank for some biorthogonal wavelets of Daubechies type (\tilde{N}, N) . Displayed are the nonvanishing values [3, Table 8.2]. Note that $\sum_k \tilde{h}_k = \sum_k h_k = 1$, so that both \tilde{h}_k and h_k can be multiplied by $\sqrt{2}$ to satisfy (84).

Daub-5/3 Filter coefficients			
$\tilde{N} = 2$	k	\tilde{h}_k	h_k
$N = 2$	0	1	$+\frac{3}{4}$
	± 1	$\frac{1}{2}$	$+\frac{1}{4}$
	± 2		$-\frac{1}{8}$

Daub-9/7 Filter coefficients			
$\tilde{N} = 6$	k	\tilde{h}_k	h_k
$N = 2(??)$	0	+1.115087052456994	+0.6029490182363579
	± 1	+0.5912717631142470	+0.2668641184428723
	± 2	-0.05754352622849957	-0.07822326652898785
	± 3	-0.09127176311424948	-0.01686411844287495
	± 4		+0.02674875741080976

Table 3: Filter bank of the two default wavelets used in the JPEG-2000 standard. Note that the coefficients are scaled such that $\sum_k h_k = 1$, but $\sum_k \tilde{h}_k = 2$. Cf. <http://www.jpeg.org/public/jcd15444-1.pdf>, p. 108. Here \tilde{h}_k is denoted as the ‘‘impulse response of the low-pass synthesis filter’’, whereas h_k is the ‘‘impulse response of the high-pass synthesis filter’’.

Example 4.7 From the same class are the Daub-5/3 and Daub-9/7 wavelets, given by the filter coefficient bank in Table 3. The corresponding wavelets are used in the JPEG-2000 standard image format. They are scaled such that $\sum_k h_k = 1$ and $\sum_k \tilde{h}_k = 2$, and satisfy (84). The filter coefficients can be easily derived from Sweldens' lifting scheme⁵ without referring explicitly to the underlying biorthogonal wavelets. \square

According to [6, §4.7], the function

$$g_N(y) = \frac{1}{c_N} \int_y^\pi (\sin t)^{2N-1} dt \quad (96)$$

with $c_N = \int_0^\pi (\sin t)^{2N-1} dt$, enables us to define the function \tilde{m}_0 such that $m_0(y)\tilde{m}_0(y) = g_N(y)$. Then

$$m_0(y)\tilde{m}_0(y) + m_0(y+\pi)\tilde{m}_0(y+\pi) = 1. \quad (97)$$

Hence by (86), the identity (97) is equivalent to the duality condition

$$\int \tilde{\varphi}(x) \varphi(x-k) dx = \delta_{0k}. \quad (98)$$

The function $\tilde{\varphi}$ is even and its support is the interval $[-2N, 2N]$. Moreover, $\tilde{\varphi}$ is in the Hölder space C^r for sufficiently large N . The wavelets ψ and $\tilde{\psi}$ then are defined by (87). Writing $\psi_{jk}(x) = 2^{j/2}\psi(2^jx-k)$ and $\tilde{\psi}_{jk}(x) = 2^{j/2}\tilde{\psi}(2^jx-k)$ for $j, k \in \mathbb{Z}$, it can be proved that (ψ_{jk}) and $(\tilde{\psi}_{jk})$ are Riesz bases dual to each other, i.e., especially $\langle \psi_{jk}, \tilde{\psi}_{j'k'} \rangle = \delta_{jj'}\delta_{kk'}$. In particular, a signal $f \in L(\mathbb{R})$ can be represented both as

$$f(x) = \sum_{j,k \in \mathbb{Z}} \langle f, \tilde{\psi}_{jk} \rangle \psi_{jk}(x) \quad \text{and} \quad f(x) = \sum_{j,k \in \mathbb{Z}} \langle f, \psi_{jk} \rangle \tilde{\psi}_{jk}(x) \quad (99)$$

The subspaces $V_0 \subset L^2(\mathbb{R})$ spanned by the Riesz basis $\varphi(x-k)$, $k \in \mathbb{Z}$ and $\tilde{V}_0 \subset L^2(\mathbb{R})$ spanned by the Riesz basis $\tilde{\varphi}(x-k)$, $k \in \mathbb{Z}$, together with the requirement that $f(x) \in V_0 \Leftrightarrow f(2^jx) \in V_j$ and $f(x) \in \tilde{V}_0 \Leftrightarrow f(2^jx) \in \tilde{V}_j$, generate two multiresolutions (V_j) and (\tilde{V}_j) dual to each other. This duality is used to define the subspaces W_j and \tilde{W}_j :

$$f \in W_j \Leftrightarrow f \in V_{j+1} \text{ and } \langle f, \tilde{u} \rangle = 0 \forall \tilde{u} \in \tilde{V}_j, \quad (100)$$

as well as

$$f \in \tilde{W}_j \Leftrightarrow f \in \tilde{V}_{j+1} \text{ and } \langle f, u \rangle = 0 \forall u \in V_j. \quad (101)$$

4.4.2 The two-dimensional case

There are several ways to construct two-dimensional wavelets from given one-dimensional ones. One possibility is simply taking the tensor product of two one-dimensional wavelet basis as 2-basis, e.g., $\Psi_{jkj'k'}(x, y) = \psi_{jk}(x)\psi_{j'k'}(y)$. The resulting functions are indeed wavelets, and $(\Psi_j)_{j \in \mathbb{Z}^2}$ is a Riesz or orthonormal basis of $L^2(\mathbb{R}^2)$ if ψ_{jk} is a Riesz or orthonormal basis of $L(\mathbb{R})$, respectively. In this basis, the two variables x and y are dilated and translated separately.

For many applications, however, there is a more appropriate construction in which the dilations of the wavelet basis control both variables simultaneously. Here it is not the tensor products of wavelets

⁵http://www.ima.umn.edu/industrial/97_98/sweldens/fourth.html

which we start from, but the one-dimensional multiresolution analysis $V_j \subset V_{j+1}$, $j \in \mathbb{Z}$. We define inductively,

$$V_0 = V_0 \otimes V_0, \quad (102)$$

$$f(x, y) \in V_j \Leftrightarrow f(2^j x, 2^j y) \in V_0, \quad (103)$$

where $V_0 \otimes V_0 = \text{closure}(\text{span}\{f(x, y) = f_1(x)f_2(y) : f_1, f_2 \in V_0\})$, i.e., $V_0 \otimes V_0$ denotes the tensor product of vector spaces. Then the V_j form a multiresolution ladder $\dots, V_{-1} \subset V_0 \subset V_1 \subset V_2 \dots$ in $L^2(\mathbb{R}^2)$ satisfying Eqs. (51) – (56). Since $\varphi(x - k)$ form a Riesz basis for V_0 , the product functions

$$\Phi_{j,\mathbf{k}}(x, y) = 2^{-j} \varphi(2^{-j}x - k_1) \varphi(2^{-j}y - k_2), \quad \mathbf{k} = (k_1, k_2) \in \mathbb{Z}^2, \quad (104)$$

form a Riesz basis for V_j . As in the one-dimensional case, we define each W_j , for $j \in \mathbb{Z}$, as the orthogonal complement of V_j in V_{j-1} , such that $V_{j-1} = V_j \oplus W_j$. An interesting observation is made if we compare this decomposition with the algebraic properties of the spaces given by construction,

$$\begin{aligned} V_{j-1} &= V_{j-1} \otimes V_{j-1} = (V_j \oplus W_j) \otimes (V_j \oplus W_j) \\ &= \underbrace{(V_j \otimes V_j)}_{V_j} \oplus \underbrace{(W_j \otimes V_j) \oplus (V_j \otimes W_j) \oplus (W_j \otimes W_j)}_{W_j}. \end{aligned}$$

Thus W_j consists of three orthogonal subspaces with Riesz bases given by $\psi_{j,k_1}(x)\varphi_{j,k_2}(y)$ for $W_j \otimes V_j$, $\varphi_{j,k_1}(x)\psi_{j,k_2}(y)$ for $V_j \otimes W_j$, and $\psi_{j,k_1}(x)\psi_{j,k_2}(y)$ for $W_j \otimes W_j$. This leads us to define *three* wavelets,

$$\Psi^h(x, y) = \varphi(x)\psi(y), \quad \Psi^v(x, y) = \psi(x)\varphi(y), \quad \Psi^d(x, y) = \psi(x)\psi(y), \quad (105)$$

where h, v, d stands for “horizontal”, “vertical”, and “diagonal”, respectively. Then, for $j \in \mathbb{Z}$ given, $\{\Psi_{j,\mathbf{k}}^h, \Psi_{j,\mathbf{k}}^v, \Psi_{j,\mathbf{k}}^d : \mathbf{k} \in \mathbb{Z}^2\}$ forms a basis of W_j , whereas $\{\Psi_{j,\mathbf{k}}^h, \Psi_{j,\mathbf{k}}^v, \Psi_{j,\mathbf{k}}^d : \mathbf{k} \in \mathbb{Z}^2\}_{j \in \mathbb{Z}}$ forms a basis of $L^2(\mathbb{R}^2) = \bigoplus_j W_j$. Then the dual scaling function is $\tilde{\Phi}(x, y) = \tilde{\varphi}(x)\tilde{\varphi}(y)$, and the dual wavelets are $\tilde{\Psi}^h(x, y) = \tilde{\psi}(x)\tilde{\varphi}(y)$, $\tilde{\Psi}^v(x, y) = \tilde{\psi}(x)\tilde{\varphi}(y)$, $\tilde{\Psi}^d(x, y) = \tilde{\psi}(x)\tilde{\psi}(y)$, see [6, p. 65].

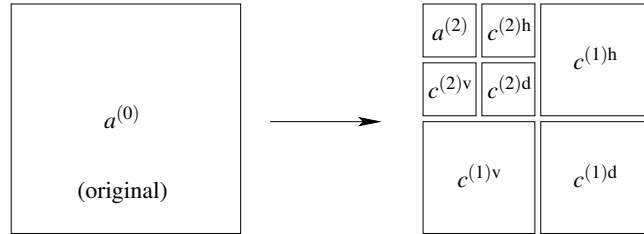


Figure 7: Visualization of the two-dimensional wavelet transform. See Figure 8.

4.5 Malvar-Wilson wavelets

To analyze a given signal, a wide class of algorithms decompose it into a linear combination of time-frequency atoms. These atoms usually are completely explicit, either given by wavelet packets or by so-called Malvar-Wilson wavelets. They are part of the general framework of windowed Fourier analysis. The window is denoted by w and allows the signal s to be cut into “slices” which are regularly spaced in time $w(t - lk)s(t)$, where $k \in \mathbb{Z}$ and l denotes the nominal length of the slices. This section follows the outline given in [6, §6.3].

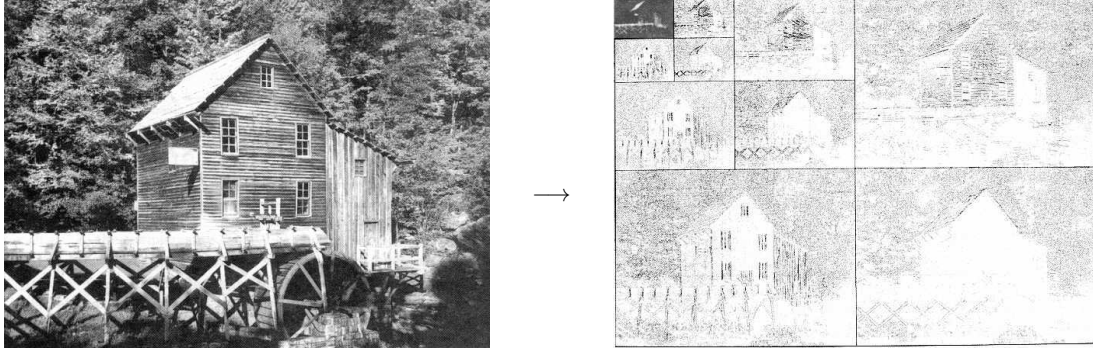


Figure 8: An image and its wavelet decomposition. The wavelet components c^h , c^v , c^d emphasize, respectively, the horizontal, vertical, and diagonal edges. Figure by courtesy of [3].

Let $n = 1$ and $(a_j)_{\mathbb{Z}}$ be a sequence with $a_j < a_{j+1}$ and $\lim_{j \rightarrow \pm\infty} a_j = \pm\infty$, such that the intervals $[a_j, a_{j+1}]$ provide a partition of the real line \mathbb{R} , i.e., $\mathbb{R} = \bigcup_{-\infty}^{+\infty} [a_j, a_{j+1}]$. Write $l_j = a_{j+1} - a_j$ for the length of the j -th interval and let $\alpha_j > 0$ be small enough such that $l_j \geq \alpha_j + \alpha_{j+1}$. Then functions $w_j \in C_0(\mathbb{R})$ satisfying the conditions

$$0 \leq w_j \leq 1 \text{ for all } t \in \mathbb{R}, \tag{106}$$

$$w_j(t) = 1 \text{ if } t \in [a_j + \alpha_j, a_{j+1} - \alpha_{j+1}], \tag{107}$$

$$w_j(t) = 0 \text{ if } t \notin]a_j - \alpha_j, a_{j+1} + \alpha_{j+1}[, \tag{108}$$

$$w_j^2(a_j + \tau) + w_j^2(a_j - \tau) = 1 \text{ if } |\tau| \leq \alpha_j, \tag{109}$$

$$w_{j-1}(a_j + \tau) = w_j(a_j - \tau) = 1 \text{ if } |\tau| \leq \alpha_j, \tag{110}$$

are called *Malvar windows*. It is immediately verified that $\sum_{-\infty}^{+\infty} w_j^2(t) = 1$ for all $t \in \mathbb{R}$. A simple example of a Malvar window [3, p. 125] is

$$w_j(t) = \begin{cases} \sin \frac{\pi}{2} v\left(\frac{t-a_j+\alpha_j}{2\alpha_j}\right) & \text{if } |t-a_j| \leq \alpha_j, \\ 1 & \text{if } a_j + \alpha_j < t < a_{j+1} - \alpha_{j+1}, \\ \cos \frac{\pi}{2} v\left(\frac{t-a_{j+1}+\alpha_{j+1}}{2\alpha_{j+1}}\right) & \text{if } |t-a_{j+1}| \leq \alpha_{j+1}, \\ 0 & \text{otherwise,} \end{cases} \quad v(x) = \begin{cases} 0 & \text{if } x \leq 0, \\ \sin^2 \frac{\pi}{2} x & \text{if } 0 < x \leq 1, \\ 1 & \text{if } 1 < x. \end{cases} \tag{111}$$

Malvar windows even can be infinitely differentiable, i.e., $w_j \in C_0^\infty(\mathbb{R})$. A *Malvar-Wilson wavelet* u_{jk}

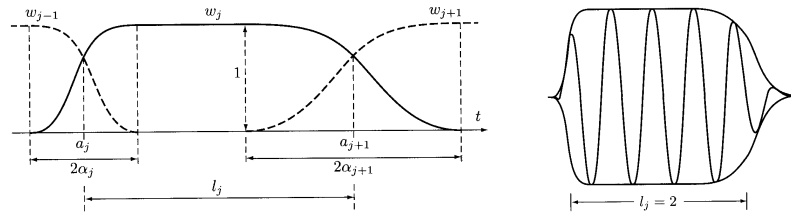


Figure 9: Malvar windows (left) and a Malvar-Wilson wavelet u_{jk} with $k = 8$ (right). Figures taken from [6].

for $j \in \mathbb{Z}$ and $k \in \mathbb{N}_0$ is then defined as

$$u_{jk}(t) = \sqrt{\frac{2}{l_j}} w_j(t) \cos \left[\frac{\pi}{l_j} \left(k + \frac{1}{2} \right) (t - a_j) \right]. \tag{112}$$

The ratio $\frac{k+1/2}{l_j}$ determines the number of oscillations in the window w_j (Figure 9). The functions u_{jk} form an orthonormal basis for $L^2(\mathbb{R})$.

The Malvar-Wilson wavelets provide a time-frequency analysis, but by a suitable choice of the Malvar windows, it can result in a time-scale analysis. To this end, we define the window function $w : \mathbb{R} \rightarrow [0, 1]$ such that

$$w(x) = 0 \quad \text{if } |x| \notin]\frac{2}{3}, \frac{8}{3}[, \quad (113)$$

$$w(-x) = w(x) \quad \text{for } x \in \mathbb{R}, \quad (114)$$

$$w(2x) = w(2-x) \quad \text{for } x \in]\frac{2}{3}, \frac{4}{3}[, \quad (115)$$

$$w^2(x) + w^2(2-x) = 1 \quad \text{for } x \in]\frac{2}{3}, \frac{4}{3}[. \quad (116)$$

Then $w_j(x) = w(2^{-j}x)$ for $j \in \mathbb{Z}$ are Malvar windows with $a_j = 2^j$, $\alpha_j = \frac{1}{3}2^j$, and $l_j = \alpha_j + \alpha_{j+1} = 2^j$. Denoting $\theta = \frac{1}{\sqrt{2}}\mathcal{F}[w(x)e^{i\pi x/2}]$, we can define the Lemarié-Meyer wavelet ψ by

$$\psi(t) = \frac{1}{\sqrt{2}}\theta(\pi t). \quad (117)$$

Then $\psi_{jk}(t) = 2^{j/2}\psi(2^j t - k)$ for $j, k \in \mathbb{Z}$ form an orthonormal basis of $L^2(\mathbb{R})$. Clearly it is possible to force w to be an infinitely differentiable function, in which case ψ is a function of the Schwartz class $\mathcal{S}(\mathbb{R})$, cf. [6, §6.4].

Although very appealing, Malvar-Wilson wavelet analysis of signals using dyadic intervals may produce artifacts. For example, in speech processing a goal is to extract phonemes. However, phonemes are not subject to the condition that they begin and end on dyadic intervals.

5 Wavelet transformation

The wavelet transformation carries out a special form of analysis by shifting the original signal from the time domain into the time-frequency domain, or time-scale domain. The idea behind the wavelet transformation is the definition of a set of basis functions which allow an efficient, and informative, representation of signals. Having emerged from an advancement in time-frequency localization from the short-time (or “windowed”) Fourier analysis, wavelet theory provides facilities for a flexible analysis as wavelets “zoom” into a frequency range.

Definition 5.1 Let $\psi \in L^2(\mathbb{R}^n)$ be a wavelet. Then the *wavelet transform* of $f \in L^2(\mathbb{R}^n)$ is the function $Wf \in L^2(\mathbb{R}^+ \times \mathbb{R}^n)$ given by

$$(Wf)(a, b) = \frac{1}{\sqrt{a^n}} \int_{\mathbb{R}^n} f(x) \bar{\psi}\left(\frac{x-b}{a}\right) dx \quad (118)$$

where $\bar{\psi}$ denotes the complex conjugate of ψ . The scalar $a > 0$ is the *dilation* or *scale factor*, and $b \in \mathbb{R}^n$ is the *translation*. As a mapping $W : L^2(\mathbb{R}^n) \rightarrow L^2(\mathbb{R}^+ \times \mathbb{R}^n)$, W is called the *wavelet transformation* with respect to ψ . \square

The translation b shifts the wavelet so that $Wf(a, b)$ contains local information of f at space location $x = b$ (or at time $t = b$ if $n = 1$). The dilation a determines the area of influence, for $a \rightarrow 0$ the wavelet transformation “zooms” into the location $x = b$, while $a \gg 0$ blurs the space (or time) resolution. The wavelet transformation \mathcal{W}_1 with respect to the dilation $a = 1$ is simply the convolution of f with the wavelet, $Wf(1, b) = (f * \psi)(b)$, see Figure 10. Moreover, $|Wf(a, b)| \leq \|f\| \|\psi\|$ for each a, b , hence

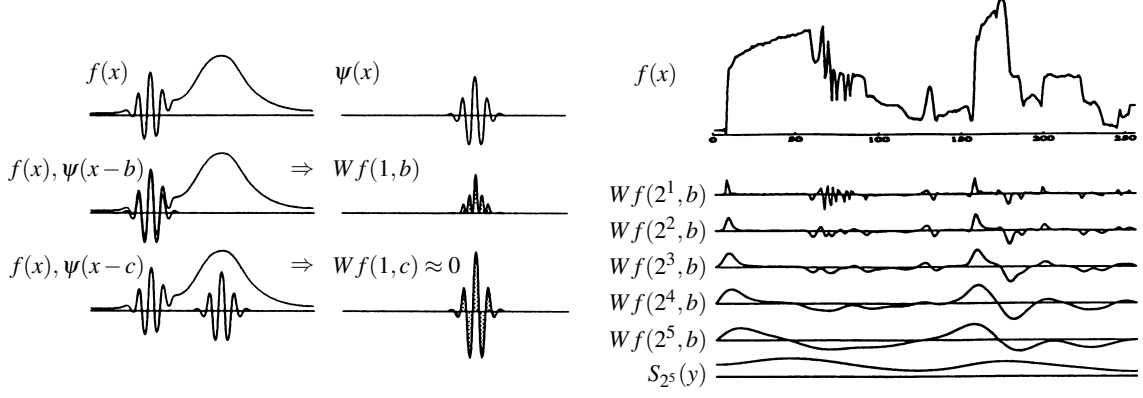


Figure 10: (a) The wavelet transformation viewed as a convolution: given a signal $f(x)$ and a wavelet $\psi(x)$, the wavelet “filters” only those frequencies which are comparable in size with its own frequency, i.e., for an appropriate y it is maximal whereas for some z it vanishes. (b) Sketch of wavelet transforms on special scales of a signal $f(x)$ with its highest frequencies represented by the wavelet ψ : the upper curve has the highest resolution and shows the finest details of the signal, the graphs below show its lower frequencies. The “remaining” frequencies are represented by $S_{2^5}(b) = \int_{2^5}^{\infty} f(x) \psi\left(\frac{x-b}{a}\right) dx \frac{da}{a^2}$.

$Wf(a, b)$ is continuous on $\mathbb{R}^+ \times \mathbb{R}^n$ [6, p. 209].

With the notion $\psi_{a,b}(x) = \sqrt{a^n} \psi\left(\frac{x-b}{a}\right)$, often called the *wavelet atoms*, the Fourier transform of $\psi_{a,b}$ is a weighted dilation of $\mathcal{F}\psi$ by $1/a$: $\mathcal{F}\psi_{a,b}(y) = \sqrt{a^n} e^{-2\pi y b} \mathcal{F}\psi(ay)$. Its center frequency is therefore y_0/a , where y_0 denotes the center frequency of the wavelet ψ .

If we introduce, for a given constant $C_\psi > 0$, the Hilbert space $L^2(\mathbb{R}^+ \times \mathbb{R}^n, db \frac{da}{C_\psi a^{n+1}})$ of functions $f : \mathbb{R}^+ \times \mathbb{R}^n \rightarrow \mathbb{C}$ and the inner product $\langle f, g \rangle_{\text{dil}} = \int_0^\infty \int_{\mathbb{R}^n} f(a, b) \bar{g}(a, b) \frac{db da}{a^2}$ such that $\|f\|_{\text{dil}} := \langle f, f \rangle_{\text{dil}} < \infty$. Then the next theorem shows that the wavelet transformation W is a “partial isometry”.

Theorem 5.2 (Partial isometry) *Let $\psi \in L^2(\mathbb{R}^n)$ be a wavelet satisfying Eq. (49) and $W : L^2(\mathbb{R}^n) \rightarrow L^2(\mathbb{R}^+ \times \mathbb{R}^n, db \frac{da}{C_\psi a^{n+1}})$ its wavelet transformation. For $f, g \in L^2(\mathbb{R}^n)$ we then have*

$$\langle Wf, Wg \rangle_{\text{dil}} = \langle f, g \rangle. \quad (119)$$

Hence $W : L^2(\mathbb{R}^n, dx) \rightarrow L^2(\mathbb{R}^+ \times \mathbb{R}^n, db \frac{da}{C_\psi a^{n+1}})$ is a partial isometry.

Proof. [3, Prop. 2.4.1]. □

Theorem 5.3 (Inversion Theorem) *Let $\psi \in L^2(\mathbb{R}^n)$ be a wavelet and $W : L^2(\mathbb{R}^n) \rightarrow L^2(\mathbb{R}^+ \times \mathbb{R}^n)$ its wavelet transformation. For $f \in L^2(\mathbb{R}^n)$ we then have the inversion formula*

$$f(x) = \frac{1}{C_\psi} \int_0^\infty \int_{\mathbb{R}^n} (Wf)(a, b) \psi\left(\frac{x-b}{a}\right) \frac{db da}{a^{n+1}} \quad (\text{a.e.}) \quad (120)$$

Proof. [6, Theorem B4]. □

We can state Theorem 5.3 in a slightly different form. A direct consequence of Theorem 5.2 and Fubini’s theorem is that $(Wf)(a, b)$ is in $L^2(\mathbb{R}^n)$ for almost all $a > 0$, and thus the function

$$f_a(x) = \frac{1}{C_\psi} \int_{\mathbb{R}^n} (Wf)(a, b) \psi\left(\frac{x-b}{a}\right) db \quad (121)$$

is well defined for almost all $a > 0$. This function f_a can be interpreted as the component of f at scale a for the decomposition given by the wavelet ψ . Then the inversion theorem states that

$$f(x) = \int_0^\infty f_a(x) \frac{da}{a^{n+1}}. \quad (122)$$

Therefore, f is the weighted sum of its components at scale a . In other words, a wavelet transformation decomposes a signal f into coefficients with respect to a given wavelet ψ . Since all wavelets live in $L^2(\mathbb{R})$, it is interesting to know whether *any* function $f \in L^2(\mathbb{R})$ can be approximated by a wavelet. Indeed, this is the case: The set of wavelets is dense in $L^2(\mathbb{R})$.

But this is only one side of the story. Even more important for practical applications, however, is the fact that for a wavelet ψ satisfying some reasonable conditions concerning decay in time and frequency [3, Prop. 3.3.2], the set $\{\psi_{2^j, 2^j n}\}_{j \in \mathbb{Z}}$ is a Hilbert basis of $L^2(\mathbb{R})$, such that

$$f = \sum_{j \in \mathbb{Z}} c_j \psi_{2^j, 2^j n}. \quad (123)$$

This means that every square integrable function can be approximated by dilated and translated version of a merely single wavelet. In the end, this property leads to the fast wavelet transformation.

For the higher-dimensional cases $n > 1$ there exist proposals to define the wavelet transform for wavelets which are not rotationally symmetric [3, §2.6]. For instance, in two dimensions we can introduce rotations in addition to dilations and translations, i.e., a third parameter θ besides a and b , the wavelet transform is given by

$$Wf(a, b, \theta) = \frac{1}{\sqrt{a^n}} \int_{\mathbb{R}^2} f(x) \psi \left(R_\theta^{-1} \cdot \frac{x-b}{a} \right) dx, \quad \text{with } R_\theta = \begin{pmatrix} \cos \theta & -\sin \theta \\ \sin \theta & \cos \theta \end{pmatrix}, \quad (124)$$

where $a \in \mathbb{R}^+$, $b \in \mathbb{R}^2$, $\theta \in [0, 2\pi[$. The inversion formula (120) then reads

$$f(x) = \frac{1}{C_\psi} \int_0^\infty \int_{\mathbb{R}^2} \int_0^{2\pi} (Wf)(a, b, \theta) \psi \left(R_\theta \frac{x-b}{a} \right) d\theta db \frac{da}{a^3} \quad (\text{a.e.}) \quad (125)$$

5.1 The image space of a wavelet transformation

Considering the wavelet transformation $W : L^2(\mathbb{R}^n) \rightarrow L^2(\mathbb{R}^+ \times \mathbb{R}^n)$ as defined in (118), is it surjective? In fact, the image $\mathcal{H} := WL^2(\mathbb{R}^n)$ of the wavelet transformation is only a subspace of $L^2(\mathbb{R}^+ \times \mathbb{R}^n)$, not the entire space. Thus for any $F \in \mathcal{H}$, we can find a function $f \in L^2(\mathbb{R}^n)$ so that $F = Wf$. It follows then that

$$F(a, b) = \int_0^\infty \int_{\mathbb{R}^n} (Wf)(a', b') \overline{W\psi_{a,b}}(a', b') \frac{db da}{C_\psi a^{n+1}} = \int_0^\infty \int_{\mathbb{R}^n} K(a, b; a', b') F(a', b') \frac{db da}{C_\psi a^{n+1}} \quad (126)$$

with

$$K(a, b; a', b') = \overline{(W\psi_{a,b})}(a', b') = \langle \psi_{a', b'}, \psi_{a, b} \rangle, \quad \psi_{a, b}(x) = \sqrt{a^n} \psi \left(\frac{x-b}{a} \right). \quad (127)$$

Since Eq. (126) can be rewritten as $F(x) = \int K(x, y) F(y) dy$, the integral kernel K is called a *reproducing kernel*, and the space \mathcal{H} is called a *reproducing kernel Hilbert space* (rk Hilbert space). An important rk Hilbert space is the space \mathcal{B}_Ω of bandlimited functions $f \in L^2(\mathbb{R}^n)$ such that $\mathcal{F}f$ has compact support, i.e., $\mathcal{F}f(y) = 0$ for $|y| > \Omega$. Here the kernel is $K(x, y) = \frac{\sin \Omega(x-y)}{\pi(x-y)}$ [3, §2.2]. In this particular case, there even exists an orthonormal basis $e_n = K(x_n, y)$ with $x_n = \frac{n\pi}{\Omega}$ which leads to Shannon's formula $f(x) = \sum_n f \left(\frac{n\pi}{\Omega} \right) \frac{\sin(\Omega x - n\pi)}{\Omega x - n\pi}$. However, such special x_n need not exist in a general rk Hilbert space.

6 Sweldens' lifting scheme

A different technique to construct biorthogonal wavelets and multiresolution analysis is the *lifting scheme* [11]. It works on discrete samples of a signal. The main difference to the classical construction presented above is that lifting does not rely on the Fourier transform and can be used to construct wavelets which are not necessarily translations and dilations of a mother wavelet.

The lifting scheme is a recursive algorithm consisting of coefficients a_k of the scaling function and c_k of the wavelets, just as in the Daubechies wavelet transform. Its basic idea is to retain in each recursion step r , as far as possible, only the even samples of the previous step coefficients $a_k^{(r-1)}$ as *approximations* $a_k^{(r)}$, and to store the *details* as wavelet coefficients $c_k^{(r)}$ in such a way that the original signal can be reconstructed uniquely. As an important example, we consider the special lifting-based transform

$$\boxed{\begin{aligned} c_k^{(r)} &= a_{2k+1}^{(r-1)} - \frac{1}{2} \left(a_{2k}^{(r-1)} + a_{2k+2}^{(r-1)} \right), \\ a_k^{(r)} &= a_{2k}^{(r-1)} + \frac{1}{4} \left(c_{k-1}^{(r)} + c_k^{(r)} \right) \end{aligned}} \quad (128)$$

Here the details c_k measure the deviation of a linear prediction and are used to “lift” the approximations of the even samples. Expressing this lifting-based transform as high-pass and low-pass filters, we see that a detail coefficient c_k is influenced by three signal coefficients a_k of the next finer level, while an approximation coefficient a_k is influenced by five coefficients of the next finer level. The high-pass (analysis) filter coefficients \tilde{h} and the low-pass (analysis) filter coefficients therefore are given by

$$\begin{array}{c|ccccc} \tilde{h}_k & 0 & -\frac{1}{2} & 1 & -\frac{1}{2} & 0 \\ \hline h_k & -\frac{1}{8} & \frac{1}{4} & \frac{3}{4} & \frac{1}{4} & -\frac{1}{8} \end{array} \quad (129)$$

These are the filter coefficients of the Daub-5/3 wavelet used in the JPEG-2000 image format standard, cf. Example 4.7.

In general, the implementation of the lifting scheme has some advantages over the implementation of the usual discrete wavelet transform. First, it reduces the number of floating point operations, in special cases it can even be implemented with pure integer operations (which are faster than floating point operations). Second, it allows an in-place calculation, i.e., the original signal can be replaced by its wavelet transform without using any additional auxiliary memory space.

7 Chirplets and the wavelet transformation

Let $H^2(\mathbb{R})$ be the *Hardy space* of class $p = 2$ consisting of the functions $f \in L^2(\mathbb{R})$ whose holomorphic extensions $f(x + iy)$ to the complex upper half-plane $\mathbb{P}^+ = \{x + iy : y > 0\}$ satisfy the condition

$$\sup_{y>0} \left(\int_{-\infty}^{\infty} |f(x + iy)|^2 dx \right)^{1/2} < \infty. \quad (130)$$

When this condition is satisfied, the upper bound taken over $y > 0$ is also the limit as $y \rightarrow 0$. The space $H^2(\mathbb{R})$ is a closed subspace of $L^2(\mathbb{R})$.

Hardy spaces play a fundamental role in signal processing. To a real-valued signal f being defined for all $t \in \mathbb{R}$ of finite energy, one associates the analytic signal F such that $f(t) = \operatorname{Re} F(t)$. By hypothesis, $f \in L^2(\mathbb{R})$, hence $F \in H^2(\mathbb{R})$. Then $F(t) = f(t) + ig(t)$. (The function g is the “Hilbert

transform" of f , i.e., $g = Hf$ with $(Hf)(x) = \frac{1}{\pi} \int_{-\infty}^{\infty} \frac{f(t)}{x-t} dt$; since $\|Hf\|_2 = \|f\|_2$ and $H(Hf) = -f$, H is an L^2 -isometry of period 4, just like the Fourier transformation.)

A *chirp* is a function $f \in L^2(\mathbb{R})$ of the form $f(t) = A(t) \cos \varphi(t)$ resulting from the corresponding analytic signal $F \in H^2(\mathbb{R})$ given by $F(t) = A(t)e^{i\varphi(t)}$, where the *modulus* A and the *argument* φ of the chirp are real-valued, belong to $C^\infty(\mathbb{R})$, and satisfy the conditions

$$\left| \frac{A'(t)}{A(t)\varphi'(t)} \right| \ll 1, \quad \left| \frac{\varphi''(t)}{(\varphi'(t))^2} \right| \ll 1. \quad (131)$$

The function $\omega(t) = \frac{\varphi'(t)}{2\pi}$ then defines the instantaneous frequency of the chirp, and the local pseudoperiod is given by its inverse $2\pi/\varphi'(t)$. By conditions (131), both the modulus $A(t)$ and the pseudoperiod vary slowly on a scale given by the local pseudoperiod $2\pi/\varphi'(t)$. In the sequel, we will simply identify f and F for convenience.

A *linear chirp* is a signal $f(t) = e^{i(\alpha t + \beta t^2)}$, $\alpha, \beta \in \mathbb{R}$, an *exponential chirp* is a signal $f(t) = e^{ik^t}$, with $n \in \mathbb{N}$, and a *hyperbolic chirp* is a signal $f(t) = e^{i\lambda \log t}$, with $\lambda \in \mathbb{R}$.

A *chirplet* is a windowed portion of a chirp $f(t)$,

$$\psi_j(t) = w_j(t)f(t). \quad (132)$$

For instance, w_j may be a Malvar window (yielding chirplets with compact supports), or the Gaussian window centered at t_j .

Example 7.1 Einstein's theory of general relativity predicts gravitational waves. In fact, they still have not been observed to date. One of the processes which is expected to generate comparatively strong gravitational waves is the collapse of binary stars. In this case the analytical description is given explicitly by a signal

$$f(t) = (t - t_0)^{-1/4} \cos\left(\omega(t_0 - t)^{5/8} + \theta\right), \quad (133)$$

where t_0 is the time when the collapse occurred, θ is a parameter, and ω is a large constant depending on the masses of the two stars. Since there is great scientific interest in detecting gravitational waves, such signals are ideal for testing and comparing various time-frequency algorithms. For a signal (133), both conditions (131) simply become $|t - t_0| \gg \omega^{-8/5}$.

For $t_0 = 0$, a segmentation of the half-line $[t_0 = 0, \infty[$ is given by $t_k = c\omega^{-5/8}k^{24/5}$ where $k = 1, 2, \dots, k_0 = c^{-1/6}\omega^{1/3}$. This means that the size of the segmentation step ranges from $\omega^{-1/3}$ to $\omega^{-8/5}$ when t reaches $t_0 = 0$, which is when the star has collapsed. For further references see [6, §6.11]. \square

A wavelet technique proposed by Innocent and Torr sani for detecting chirps, especially described by (133), bases on a "ridge" detection. The "ridge" is a region near $b = t_0$ where the wavelet transform of a chirp will be large. Consider the chirp $f(t) = A(t)e^{i\varphi(t)}$. Its wavelet transform

$$Wf(a, b) = \frac{1}{a} \int f(t) \psi\left(\frac{t-b}{a}\right) dt \quad (134)$$

will be small due to cancellations, if the chirp and the wavelet do not oscillate with the same frequency. By the same reasoning, the wavelet transform will be large if the pseudoperiod $2\pi/\varphi'(b)$ coincides with the pseudoperiod a of the wavelet. Thus the wavelet transform will be large near the curve

defined by $a = 2\pi/\varphi'(b)$. There is no cancellation on this curve, and the computation of the wavelet transform goes like this:

$$Wf(a,b) = \frac{1}{a} \int f(t) \psi\left(\frac{t-b}{a}\right) dt \approx \frac{1}{a} \int |f(t)| \left| \psi\left(\frac{t-b}{a}\right) \right| dt = \frac{1}{a} \int A(t) \left| \psi\left(\frac{t-b}{a}\right) \right| dt.$$

In view of the first condition in (131), we expect that $A(t)$ does not vary much on the support of the wavelet, so that $\frac{1}{a} \int A(t) \left| \psi\left(\frac{t-b}{a}\right) \right| dt \approx \|\psi\|_1 A(b)$. This argument leads to the following heuristic: The continuous wavelet transform of a chirp is large in a neighborhood of the curve $a = 2\pi/\varphi'(b)$, where

$$Wf(a,b) \approx \|\psi\|_1 A(b).$$

In the case of chirps (133) generated by the collapse of binary stars, $\varphi(t) = (t - t_0)^{5/8}$ and $A(t) = (t - t_0)^{-1/4}$, and the ridge is located near the curve

$$a = \frac{16\pi}{5\omega} (t_0 - b)^{3/8}. \quad (135)$$

If we take $\|\psi\|_1 = 1$, then $|Wf(a,b)| \approx (t_0 - b)^{-1/4}$ near this curve. Therefore, the ridge depends only on the two parameters t_0 and ω , and locating the ridge in the time-frequency enable to find t_0 and to determine the characteristic mass parameter ω .

8 Vision

In cognition psychology, the currently usual model of the visual system, just as of the somatosensory system (sense of touch), can be essentially understood as a wavelet model. Let us shortly outline the process of vision. After the retina in our eye has finished its perception processing of an image, its results are sent to the optic nerve of the brain, an electric cable consisting of millions of wires, the *axons*. Many of these wires directly lead to the *lateral geniculate nucleus (nucleus geniculatus lateralis) GL*. After the having been processed by the GL, the data go through another strand of axons to the *primary visual cortex V1*.

Every neuron taking part of the visual system has its own *receptive field*, a spatially confined region in which the presence of a certain stimulus, i.e., a light pattern or spatial changes of light intensities, alters the firing of the neuron. For instance, many neurons of the GL have a receptive field as sketched in Figure 11 (a). Depending on magnitude and position of the light pattern, certain

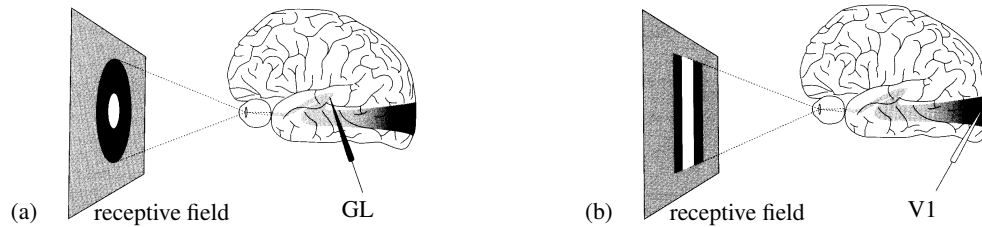


Figure 11: Light patterns on a screen as receptive fields, stimulating certain neurons. (a) Receptive field of many neurons in the GL. (b) Receptive field of many neurons in the V1.

neurons are stimulated and increase their rates of electric discharge, measurable by electrodes. In the V1, however, there are many neurons whose receptive fields consist of lines, Figure 11 (b). In other words, each region and each (visual!) light pattern in our visual field has certain neurons “watching

out” for them. About some millions of neurons in the retina and in the GL are taking part of the visual perception process, in the V1 even some hundred millions of neurons [4, §4.1.5], [5, §3].

In the wavelet model of vision, the image in front of our eyes is the signal, being composed of various receptive fields. From our own experience, we all know the analogous phenomenon of the sense of touch, where the receptive fields of the finger tips, for instance, are considerably smaller than the receptive fields of the back of the hand, so that we can feel the smoothness or coarseness of a surface much better than with the back of our hand.

What we see is therefore decomposed by our brain into different receptive fields, exactly as signals in signal processing are decomposed into wavelets. Accordingly, the reaction of a certain neuron is represented by the “wavelet coefficient”. If a neuron is not stimulated, its wavelet coefficient is zero, if it is excited strongly and fires often, its wavelet coefficient is large. Just like a wavelet transform, small receptive fields encode small scales (causing a high resolution, high detail accuracy, good spatial localization), and large receptive fields encode large scales (giving rise to a bad spatial resolution, but a well-defined frequency).

8.1 Marr’s program

In the 1970’s, a group led by Marvin Minsky at the MIT artificial intelligence laboratory worked on artificial vision for robots. The goal was to construct a robot endowed with a perception of its environment. The first attempts to solve the problem were disappointing to the robot scientists, such that David Marr, a British expert on the human visual system, was invited to join the group. Starting from the observation that it was not pure imitation of Nature, such as copying the forms of birds or the structures of feathers, which led to the construction of aeroplanes, but the understanding of the *laws* of aerodynamics governing the flight of birds, he developed a model of vision which underlies both the human visual system as well as computer vision. He identified four crucial steps of human vision:

1. The recognition of contours of objects. These are the contours which delimit objects and in this way structure the environment into distinct objects.
2. The sense of the third dimension from two-dimensional retinal images and the ability to obtain a three-dimensional organization of physical space.
3. The extraction of reliefs from shadows.
4. The perception of motion in an animated scene.

From this he states that a theory of vision has to answer the following fundamental questions:

1. How can the contours of objects be scientifically defined by the variations of their light intensity?
2. How is it possible to sense spatial depth?
3. How is motion perceived? How do we recognize that an object has moved by examining a succession of images?

Marr’s working hypothesis was that human vision and computer vision are basing on the same principles, so that algorithmic answers to these questions can be tested within the framework of artificial vision. If such algorithms work for computers, it can be investigated whether and how they can be

implemented physiologically. For instance, Marr doubts that human neuronal circuits use iterative loops which are an essential part of existing computational algorithms.

The central question of the actual physiological implementation is the *representation* of the information on which the vision algorithms rely on. The kind of representation has significant consequences on the algorithm itself. To take an elementary example, the algorithm to multiply two integers are considerably different for the representation in the decimal system and the Roman number system.

8.2 Edge recognition by zero-crossings

According to Marr, the image processing in the human visual system has a hierarchical structure involving several layers of processing. One of the first layers yields the “raw primal sketch” of the image, furnished by the retinal system as a succession of sketches at different scales in geometric progression. These sketches are made with lines, and they are recognized by the *zero-crossings* of the second derivative of the intensity distribution function f , since they locate the minima and maxima of the intensity change (i.e., the first derivative of f). In order to detect intensity changes efficiently, Marr suggests that the visual system at these stages uses a filter which takes the first and second derivative of the intensity distribution of the image, and in addition is capable to act on different scales, so that large filters can be used to detect blurry shadow edges and small filters to detect fine details in the image. In [7] the wavelet

$$\psi_\sigma(x, y) = -\frac{1}{\pi\sigma^4} \left(1 - \frac{x^2 + y^2}{2\sigma^2}\right) e^{-(x^2 - y^2)/2\sigma^2}, \quad (136)$$

is proposed, today called *Marr's wavelet* or *Mexican hat wavelet*. We have $\psi_\sigma(x, y) = \Delta G(x, y)$ where $\Delta = \frac{d^2}{dx^2} + \frac{d^2}{dy^2}$ is the Laplacian and G is the two-dimensional Gaussian density $G(x, y) = \frac{1}{2\pi\sigma^2} e^{-(x^2 + y^2)/2\sigma^2}$.

Suppose a black and white image is represented by the gray levels $f(x, y)$ in its pixel points $(x, y) \in \mathbb{Z}^2$. Then the zero-crossings are given by the zeros of the convolution of f with the wavelet ψ_σ , i.e., $(f * \psi_\sigma)(x, y) = 0$. Since ψ is even, $\psi(-x, -y) = \psi(x, y)$, the values of the convolution $f * \psi_\sigma$ are, up to a constant, the wavelet coefficients of f , analyzed with ψ . In other words, the zero-crossings of the image are determined by the vanishing of the wavelet coefficients,

$$W_\psi f(\sigma; x, y) = 0, \quad \psi(x, y) = -\frac{1}{\pi} \left(1 - \frac{x^2 + y^2}{2}\right) e^{-(x^2 - y^2)/2}, \quad (137)$$

The values for σ used in human vision are in geometric progression, and experiments lead the values

$$\sigma_j = \left(\frac{7}{4}\right)^j \sigma_0; \quad (138)$$

for details and further references see [6, §8.2]. Marr conjectured that the original image is *completely* determined by the sequence of curve lines $(f * \psi_{\sigma_j})(x, y) = 0$. Formulated in this generality, the conjecture is false, since there is known a counterexample consisting for periodic images covering an unbounded area [6, §8.3]. However, it is still open today whether the conjecture is true or false for images of finite extent.

From the point of view of current computer vision research, the Marr-Hildreth approach suffers from two main limitations. First, it generate responses that do not correspond to edges, so-called “false edges”, and second, the localization error may be severe at curved edges. Among the currently mostly used edge detection methods is the Canny algorithm based on the search for local directional

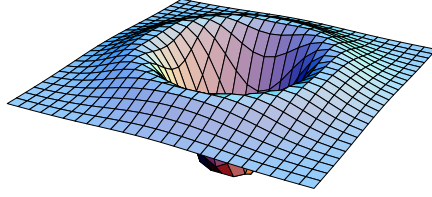


Figure 12: The Marr, or Mexican hat, wavelet.

maxima in the gradient magnitude, or the differential approach based on the search for zero-crossings of the differential expression that corresponds to the second-order derivative in the gradient directions.

A remarkable property of the Marr-Hildreth edge detection algorithm is that it always forms connected closed contours, despite contours leaving the edge of the image. This comes, however, at the expense of localization, especially for larger values of σ . The Canny edge detection does better localization, especially for larger values of σ , but the edge segments can become disconnected.

8.3 Mallat's algorithm

Stéphane Mallat generalized Marr's approach by replacing the Gaussian by the basic cubic spline θ with compact support $[-2, 2]$, which is given as the convolution $\theta = T * T$ where T is the triangle function $T(x) = 1 - |x|$ if $|x| \leq 1$, and $T(x) = 0$ if $|x| > 1$, cf. Figure 13 (b), and Example 4.4. θ is called the *smoothing function*. Let f be the signal function we wish to analyze by the method of

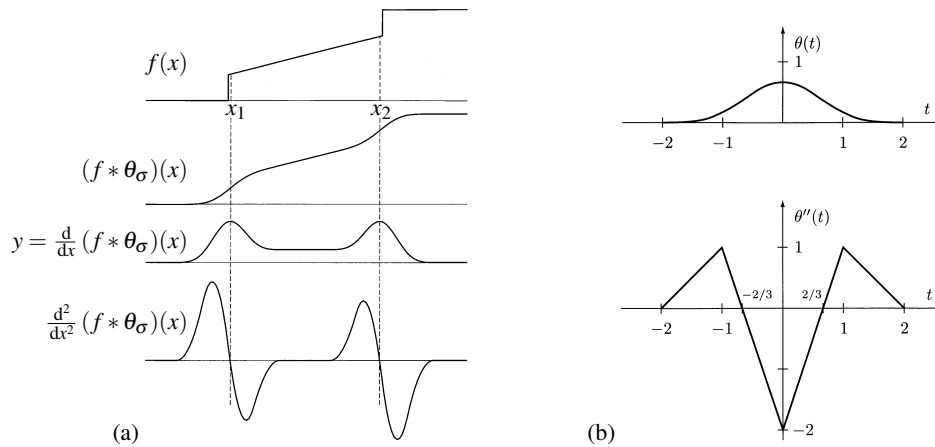


Figure 13: (a) Mallat's algorithm. (b) The cubic spline $\theta = T * T$ and its second derivative θ'' . Figures taken from [6] ©SIAM

zero-crossing, and define $\theta_\sigma(x) = \sigma^{-1}\theta(\sigma^{-1}x)$. Then the zero-crossings are the values of x where the second derivative satisfies $\frac{d^2}{dx^2}(f * \theta_\sigma)(x) = 0$ and changes sign. To use the “pyramid algorithm”, Mallat proposes to stick to the dilations $\sigma = 2^{-j}$, $j \in \mathbb{Z}$, and to code the signal $f(x)$ with the double sequence $(x_{q,j}, z_{q,j})$ where

- (a) $x = x_{q,j}$ is a zero-crossing of $\frac{d^2}{dx^2}(f * \theta_{2^{-j}})$, and
- (b) $z_{q,j} = \frac{d}{dx}(f * \theta)(x_{q,j})$.

In other words, the double sequence contains the (x, y) -values of the local extrema of the first derivative $\frac{d}{dx}(f * \theta)$. Some of these local extrema are related to points where the signal f changes rapidly,

i.e., where $|z_{q,j}| \gg 0$, such as x_1 and x_2 in Figure 13 (a). Only these values are retained, the other values are ignored. One realization of this idea is to use a certain threshold value $z_{\min} > 0$, so that only those zero crossings satisfying $|z_{q,j}| \gg z_{\min}$ are stored.

Can an arbitrary image, determined by a compactly supported signal function f and filtered by Mallat's algorithm, be completely reconstructed? In this generality, the answer is no.

Example 8.1 (*Meyer's counterexample*) A counterexample due to Meyer [6, §C] is the signal function $f(t) = f_0(t) + g'''(t)$, with

$$f_0(t) = \begin{cases} 1 + \cos t & \text{if } |t| \leq \pi, \\ 0 & \text{if } |t| > \pi, \end{cases} \quad g(t) = \begin{cases} -h(-t) & \text{if } 0 \leq t, \\ h(t) & \text{if } \frac{\pi}{8} \leq t < \frac{\pi}{4}, \\ 0 & \text{otherwise,} \end{cases} \quad (139)$$

where $h \in C_0^\infty(\mathbb{R})$ is an arbitrary function with support in $[\frac{\pi}{8}, \frac{\pi}{4}]$. □

However, there are two ways to save Mallat's algorithm and to guarantee perfect reconstruction. The first way is to take another smoothing function θ , for instance the *Tukey window*

$$\theta(t) = \begin{cases} 1 + \cos t & \text{if } |t| \leq \pi, \\ 0 & \text{if } |t| > \pi. \end{cases} \quad (140)$$

With this choice, any real-valued function $f \in C_0^\infty(\mathbb{R}) \cap L^1(\mathbb{R})$ can be uniquely reconstructed from knowing the values $(x_{q,-j}, y_{q,-j})_{j \in \mathbb{N}}$ [6, Theorem C.1].

The second way to let Mallat's algorithm work correctly is to restrict the set of signal functions f to be analyzed. If, for instance, f is a step function with an arbitrarily large number of discontinuities, then it is reconstructed perfectly by the sequence $(x_{q,j}, z_{q,j})_{q,j \in \mathbb{Z}}$ [6, §8.4]. Since in any digital signal in fact is a step function with finitely many discontinuities, and also any image being processed by the retina cells consists of step function signals, this restriction even is reasonable in practice both for human as well as computer vision.

8.3.1 Mallat's algorithm in two dimensions

Suppose $f \in L^2(\mathbb{R}^2)$ is a signal caused by a two-dimensional image. From this we create the increasingly blurred versions at scales $\sigma_j = 2^{-j}$, $j \in \mathbb{Z}$, by taking the convolutions $f * \theta_{\sigma_j}$, where

$$\theta_\sigma(x, y) = \theta_\sigma(x)\theta_\sigma(y). \quad (141)$$

Here $\theta(\cdot)$ denotes the basic cubic spline as used above in the one-dimensional case.

Next we consider the local maxima of the modulus of the gradient of $f * \theta_{\sigma_j}$, i.e., $|\nabla(f * \theta_{\sigma_j})|(x_q, y_q)$, where $\nabla = \left(\frac{d}{dx}, \frac{d}{dy}\right)$. Here the zero-crossings are given by the points $(x_q, y_q) \in \mathbb{R}^2$ where the Laplacian vanishes,

$$\Delta(f * \theta_{\sigma_j})(x_q, y_q) = 0, \quad (142)$$

with $\Delta = \frac{d^2}{dx^2} + \frac{d^2}{dy^2}$, and where additionally there exist points $(x_\pm(r), y_\pm(r))$ on *each* circle around (x_q, y_q) with radius $r < \varepsilon$ for some $\varepsilon > 0$ such that

$$\Delta(f * \theta_{\sigma_j})(x_\pm(r), y_\pm(r)) \geq 0. \quad (143)$$

In case of an image given by discrete pixels, this condition is equivalent to the criterion that the Laplacian of at least one of the eight pixels surrounding the pixel (x_q, y_q) is negative, and at least one is positive. The positions (x_q, y_q) of these zero-crossings, as well as the values of the gradients at these points, $(z_{1,q}, z_{2,q}) = \nabla(f * \theta_{\sigma_j})(x_q, y_q)$, are then stored in memory.

References

- [1] Walter Appel. *Mathématiques pour la physique et les physiciens*. H&K Éditions, Paris, 3 edition, 2005.
- [2] Ingrid Daubechies. Orthonormal bases of compactly supported wavelets. *Comm. Pure and Applied Mathematics*, XLI(8):909–996, 1988.
- [3] Ingrid Daubechies. *Ten Lectures on Wavelets*. Society of Industrial and Applied Mathematics, Philadelphia, 1992.
- [4] Rainer Guski. *Wahrnehmen — ein Lehrbuch*. W. Kohlhammer, Stuttgart Berlin Köln, 1996.
- [5] Donald D. Hoffman. *Visuelle Intelligenz. Wie die Welt im Kopf entsteht*. Cotta'sche Buchhandlung, Stuttgart, 2000.
- [6] Stéphane Jaffard, Yves Meyer, and Robert Dean Ryan. *Wavelets. Tools for Science and Technology*. Society for Industrial and Applied Mathematics, Philadelphia, 2001.
- [7] D. Marr and E. Hildreth. Theory of edge detection. *Proc. Roy. Soc. London Ser. B*, 207:187–217, 1980.
- [8] Yves Nievergelt. *Wavelets Made Easy*. Birkhäuser, Boston Basel Berlin, 1999.
- [9] William H. Press, Saul A. Teukolsky, William T. Vetterling, and Brian P. Flannery. *Numerical Recipes in C++. The Art of Scientific Computing*. Cambridge University Press, Cambridge, 2 edition, 2002.
- [10] Howard L. Resnikoff and Raymond O. Wells. *Wavelet Analysis. The Scalable Structure of Information*. Springer-Verlag, New York, 1998.
- [11] Wim Sweldens. The lifting scheme: a custom-design construction of biorthogonal wavelets. *Applied and Computational Harmonic Analysis*, 3(2), 1996.

Web-Links

- [Abb] <http://wolframcloud.com/obj/abbott/Published/D4Rationals.nb> – Abbott, Paul C.: Wolfram Notebook computing Daubechies wavelets for scaling function $\varphi(\frac{1}{3})$
- [L1] <http://www.cmap.polytechnique.fr/~bacry/LastWave/> – LastWave, a C-programmed signal processing oriented command language